

Mechanical Vibration Effects on Enhanced Melting of Phase Change Materials within Latent Heat Thermal Energy Storage Devices Under Different Container Orientations

By

Haohua Xiao

A thesis submitted to the Graduate Faculty of

Auburn University

in partial fulfillment of the

requirements for the Degree of

Master of Science

Auburn, Alabama

December 2023

Approved by

Jay M. Khodadadi, Chair, Professor, Mechanical Engineering

Daniel Harris, Associate Professor, Mechanical Engineering

Nicholas Tsolas, Assistant Professor, Mechanical Engineering

Abstract

Phase change materials (PCM) are playing a bigger role in our daily life, from cooling of electric vehicle batteries to spacecrafts in the outer space. Research on PCM melting behavior and system performance has generally focused on cases without mechanical vibrations, whereas practical latent heat thermal energy storage (LHTES) units incorporating PCM are subjected to uncontrollable mechanical vibrations. An instrumented rectangular LHTES unit that incorporates a heated plate connected to two aluminum end plates normal to the heated plate was built. The remaining two plates were made of Plexiglas to accommodate visual observations. In effect, the PCM was held in the space defined by the aluminum-Plexiglas side walls. The set-up can be oriented as needed with respect to the gravitational field. Two sets of experiments corresponding to (i) no mechanical vibrations and (ii) mechanical vibrations were conducted.

For cases with no mechanical vibrations, melting experiments corresponding to the inclination angles of 90, 60, 45, 30 and 0 degrees were conducted. For the inclination angle of 90 degrees (horizontal heater plate at bottom), expedited melting was observed next to the two aluminum walls, whereas wavy liquid-solid interface (LSI) was present in the vicinity of the mid-plane signifying presence of a thermally-unstable layer. It was also noted that strong three-dimensionality of the liquid-solid interface was persistent contrary to information available at the observation plane. Temperature recordings on both heat conducting aluminum walls also exhibited lack of plane symmetry. As the inclination angle was raised, distinction among thermocouples readings among the two batches were clearly observable. For the inclination angle of 0 degrees (vertical heater plate), the wavy liquid-solid interface was observed next to the bottom heated aluminum plate where a thermally-unstable layer is present. Among the cases with no vibration, the melting rate based on the estimation of the LSI at the observation window has increased as

many as 45% with the increase of the vibration frequency. In explaining the LSI waviness, the effect of the Rayleigh number on intensification of the thermally unstable layer being formed between the bottom heated aluminum plate and the receding PCM's liquid-solid interface was elucidated.

The unit was also subjected to mechanical vibrations at an acceleration level of 1 g subject to 50 and 100 Hz for the inclination angle of 0 degrees. In view of greater leakage of liquid from the unit, observing melting enhancement is promising.

Table of Contents

| | |
|---|-----|
| Abstract | 2 |
| List of Tables..... | 5 |
| List of Figures..... | 6 |
| Chapter 1 Introduction | 10 |
| Chapter 2 Literature Review | 13 |
| Chapter 3 Experimental Set-up and Procedures | 24 |
| Chapter 4 Experimental Results | 33 |
| Chapter 5 Conclusions and Recommendations..... | 91 |
| References | 93 |
| Appendix A Thermocouple Preparation and Calibration | 94 |
| Appendix B Preparation of the PCM Container | 101 |
| Appendix C PCM Filling Process | 105 |
| Appendix D Building and Assemble the Final Test Bench | 112 |
| Appendix E Thermocouple Testing Bead Shape Effect and Size Effect | 114 |
| Appendix F Thermocouple Wire Length Effect | 116 |
| Appendix G Effect by Location of Thermocouple Beads | 117 |

List of Tables

Table 2.1 Summary of the operating features of the mechanical vibration studies.

Table 3.1: 99% Octadecane Technical Detail

Table 3.3: Sample calculation of getting the acceleration

List of Figures

Figure 1.1: CSP that converts solar irradiation into electricity utilizing a recirculating salt to store energy via sensible heat (Bošnjaković and Tadijanović, 2019).

Figure 2.1: Figure 2.1 Schematic diagram of the experimental test section (Henze and Humphrey, 1981)

Figure 2.2: Instantaneous evolution of the LSI during experiments with finned system (Henze and Humphrey, 1981)

Figure 2.3: Flow visualization of natural convection-induced recirculatory vortex (Eftekhar *et al.*, 1984)

Figure 2.4: Experimental test-section of Scammell (2011)

Figure 2.5: Time-varying progression of the LSI away from the vertical heated surface for case (a) without metal foam and (b) with metal foam (Scammell, 2011)

Figure 2.6 Experimental set-up of Vadasz *et al.* (2016) for solidification of paraffin stored within plastic spheres subjected to vertical vibrations

Figure 2.7: Components of the experimental set-up of Joshy *et al.* (2020)

Figure 2.8: Experimental set-up of Lee and Han (2022)

Figure 3.1: Schematic diagram of the experimental set-up

Figure 3.2: Photograph of the instrumented experimental set-up and various measurement components

Figure 3.3: Thermocouple Locations (note matching of the vertical positions of some thermocouple pairs, i.e., 2 & 7, 4 & 9, 5 & 11)

Figure 3.4: Vibration Table Set-Up

Figure 4.1 Instantaneous progression of the liquid-solid interface on the front observation window of the set-up during melting without vibration for the inclination angle of 90 degrees (horizontally-oriented heated plate at the bottom)

Figure 4.2: Slanted View for the Evidence of 3-Dimensional Melting ($t > 30$ minutes)

Figure 4.3: Temperature variations with time during Melting Without Vibration for the inclination angle of 90 degrees (horizontally-oriented heated plate at the bottom)

Figure 4.4: Instantaneous progression of the liquid-solid interface on the front observation window of the set-up during Melting Without Vibration for the inclination angle of 60 degrees

Figure 4.5: Temperature variations with time during Melting Without Vibration for the inclination angle of 60 degrees

Figure 4.6: Instantaneous progression of the liquid-solid interface on the front observation window of the set-up during Melting Without Vibration for the inclination angle of 45 degrees

Figure 4.7: Temperature variations with time during Melting Without Vibration for the inclination angle of 45 degrees

Figure 4.8: Instantaneous progression of the liquid-solid interface on the front observation window of the set-up during Melting Without Vibration for the inclination angle of 30 degrees

Figure 4.9: Temperature variations with time during Melting Without Vibration for the inclination angle of 30 degrees

Figure 4.10: Instantaneous progression of the liquid-solid interface on the front observation window of the set-up during Melting Without Vibration for the inclination angle of 0 degrees (vertically-oriented heated plate on the far left)

Figure 4.11: Slanted View for the Evidence of 3-Dimensional Melting ($t > 20$ minutes)

Figure 4.12: Temperature variations with time during Melting Without Vibration for the inclination angle of 0 degrees (vertically-oriented heated plate on the far left)

Figure 4.13 Estimated Melting Fraction Values without Vibration estimated from observation window images at the 30 minutes time instant

Figure 4.14 Estimated values of the Rayleigh numbers above thermocouples 7-15 for the inclination angle of 0 degrees

Figure 4.15: Multimeter Read out for voltage and current

Figure 4.16: Instantaneous progression of the liquid-solid interface on the front observation window of the set-up during Melting Without Vibration for the inclination angle of 0 degrees with Mechanical Vibration at 50 Hz (1G) (vertically-oriented heated plate on the far left)

Figure 4.17: Temperature variations with time during Melting With 50 Hz (1G) Mechanical Vibration for the inclination angle of 0 degrees (vertically-oriented heated plate on the far left)

Figure 4.18: Instantaneous progression of the liquid-solid interface on the front observation window of the set-up during Melting Without Vibration for the inclination angle of 0 degrees with Mechanical Vibration at 100 Hz (1G) (vertically-oriented heated plate on the far left)

Figure 4.19: Temperature variations with time during Melting With 100 Hz (1G) Mechanical Vibration for the inclination angle of 0 degrees (vertically-oriented heated plate on the far left)

Figure 4.20: Variations of the Heated Plate Temperatures for various inclination angles

Figure 4.21: Estimated Melting Fraction Chart with Vibration Cases

Chapter 1 Introduction

This Chapter will provide an overview of the energy storage systems that are vital to operation of renewable energy systems. Focusing on thermal energy systems, utilization of phase change materials (PCM) will be emphasized. The scope of this thesis is then outlined.

1.1 Energy Storage

Wide-spread availability and access to clean forms of energy are widely pursued to address issues related to global warming, environmental pollution, etc. Renewable forms of energy (i.e. solar, wind, ocean, etc.) are logical candidates to replace fossil fuels, thus contributing to global drive toward decarbonization. The bottleneck faced by utilization of all forms of renewable energy is the topic of energy storage. Renewable sources of energy, e.g., solar irradiation at a certain position, are intermittent. Thus, well-designed and robust thermal energy storage units must be an integral part of the system. Such a storage unit operating in a concentrating solar plant (CSP) is illustrated in Figure 1.1, where the hot and cold salt tanks are clearly identifiable. In this system, thermal energy is stored through utilization of the sensible heat thermophysical property of all materials. In effect, as the material is cooled or heated, its temperature will decline or rise.

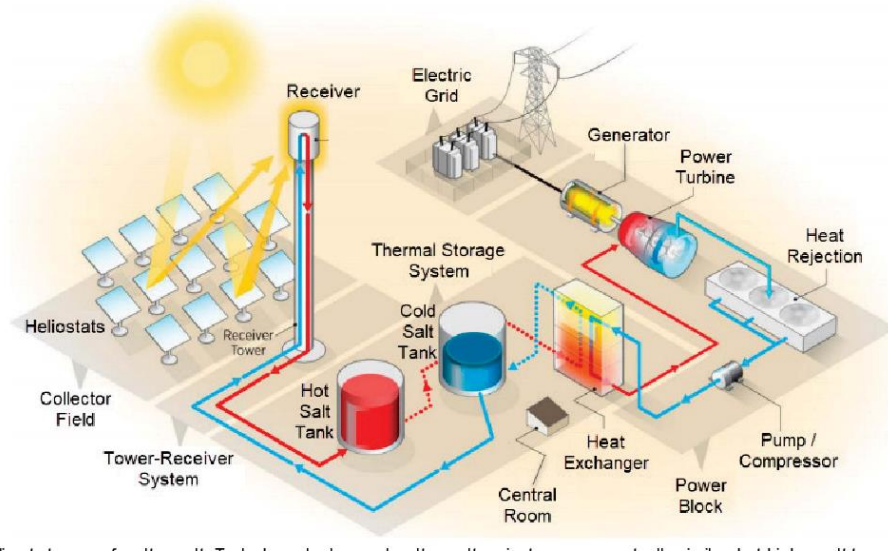


Figure 1.1: CSP that converts solar irradiation into electricity utilizing a recirculating salt to store energy via sensible heat (Bošnjaković and Tadijanović, 2019).

1.2 Latent Heat Mode of Thermal Energy Storage

Phase change materials have long been used in for a variety of purposes ranging from building materials, thermal management of electronics, textiles, spacecraft, etc. With recent years of energy crisis and ever-increasing market of fully electric vehicles, the number of research on PCM has grown dramatically. PCM store/release sizeable amounts of thermal energy at a nearly constant temperature through liquid-solid transition, commonly known as thawing-freezing cycles. This thermophysical mode of energy storage is favored when compared to the sensible heat storage approach due to lack of temperature excursions and less mass of storage media.

1.3 Effect of Mechanical Vibrations on Melting

While a lot of research was already performed towards the melting behavior of PCM, the adopted test cells were not generally subjected to controllable mechanical vibrations. Under actual operating conditions, such as electric vehicles experiencing vibrations, the performance of the PCM unit will be affected by the imposed mechanical vibrations.

1.4 Scope of Thesis

Starting with a simple PCM storage unit, a set of experiments were conducted to elucidate the role of the inclination angle on the melting pattern, progression of the liquid-solid interface (LSI) and recorded thermocouple readings under conditions with no vibrations. In this connection, there are prior research against which our results can be compared.

Mechanical vibrations were then imposed for the case of a fixed inclination angle and pertinent data were collected. In this thesis, the following chapters will be covered:

- a. Literature review pertinent to the study are discussed in Chapter 2,
- b. Experimental set-up and procedures will be presented in Chapter 3,
- c. Experimental results will be covered in Chapter 4,
- d. Conclusions and recommendations will be presented in Chapter 5.

Chapter 2 Literature Review

This chapter will focus on a summary of prior investigations reported to date in relation to effects of mechanical vibrations in latent heat thermal energy storage (LHTES) units by other researchers. However, prior to that coverage, a few references that are relevant to the experimental set-up employed in this study are discussed.

2.1 Overview of Prior Work on Rectangular LHTES Test Cells

The experimental set-up employed in this study will be summarized in Chapter 3. The set-up that was employed has been studied by some researchers earlier and this will offer an opportunity to compare our results to their findings. Moreover, the set-up allows:

- (a) versatility in orientation with respect to the gravitational acceleration,
- (b) versatility in realizing presence of thermally stable and unstable layers simultaneously within the liquid PCM.

Henze and Humphrey (1981) presented a two-dimensional heat conduction model for predicting the melting rate and liquid-solid interface of finned PCM storage devices. In order to validate their model, they designed and studied visualized melting experiments of a double-finned rectangular Plexiglas container of inside dimensions $12.70 \text{ cm} \times 2.54 \text{ cm} \times 3.18 \text{ cm}$, which was filled with octadecane (Fig. 2.1).

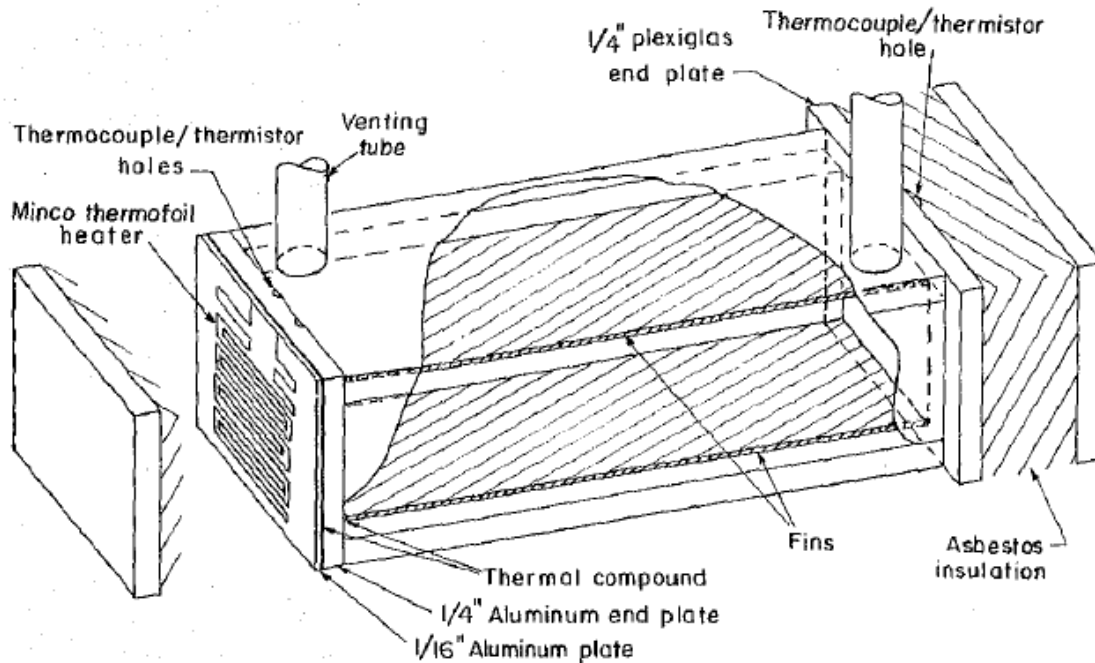


Figure 2.1: Schematic diagram of the experimental test section (Henze and Humphrey, 1981)

The research introduces a novel, simplified model that predicts the melting behavior of PCM in finned systems. The experimental data, particularly as depicted in Figure 2.2, validates the model's assumptions, such as neglecting heat conduction in the solid phase of the PCM and focusing on latent heat of fusion. This model, backed by empirical evidence, underscores the critical influence of fin geometry and spacing in PCM systems.

In essence, Henze and Humphrey's study underscores the importance of fins in thermal energy storage systems. By demonstrating how fins can significantly improve the efficiency of heat transfer in PCM, this study offers valuable insights into the design and optimization of phase-change energy storage devices. It highlights the potential for fins to transform the performance of these systems, making it a significant reference in the field of thermal energy storage.

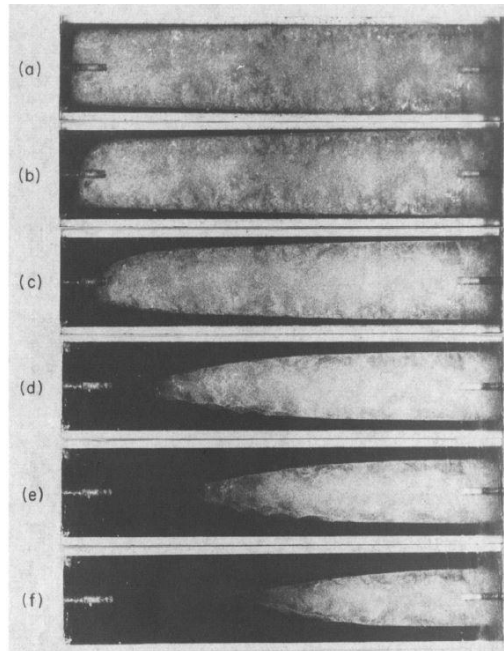


Figure 2.2: Instantaneous evolution of the LSI during experiments with finned system (Henze and Humphrey, 1981)

In general, the presence of metal fins significantly suppressed natural convection but strongly enhanced conduction. It was argued that if more fins are closely spaced, convection becomes more negligible and the proposed model can give better predictions.

The study by Eftekhar et al. (1984) investigates enhancing heat transfer in thermal storage systems using paraffin wax as a phase change material (PCM). They employ vertically arranged fins in a finned-tube setup to induce natural convection in the liquid phase of paraffin wax, which becomes highly efficient at temperatures above 50 °C. The study's primary aim is to understand the impact of natural convection on heat transfer at the liquid-solid interface, crucial for efficient latent heat storage. A key feature of the study is the experimental setup, comprising a thermal

storage device with two parallel plates separated by vertical fins, designed to handle the volumetric expansion of paraffin wax and allow flow visualization.

A significant result of the study is presented in Figure 2.3, which shows the fraction of liquid produced as a function of time. This graph is crucial as it illustrates the efficiency of the heat transfer process, highlighting the effectiveness of the system in converting solid wax to liquid. The results demonstrate that the heat transfer coefficient in this system is higher than that for convection alone, attributable to the movement of small, finite solid particles at the interface which enhances heat transfer.

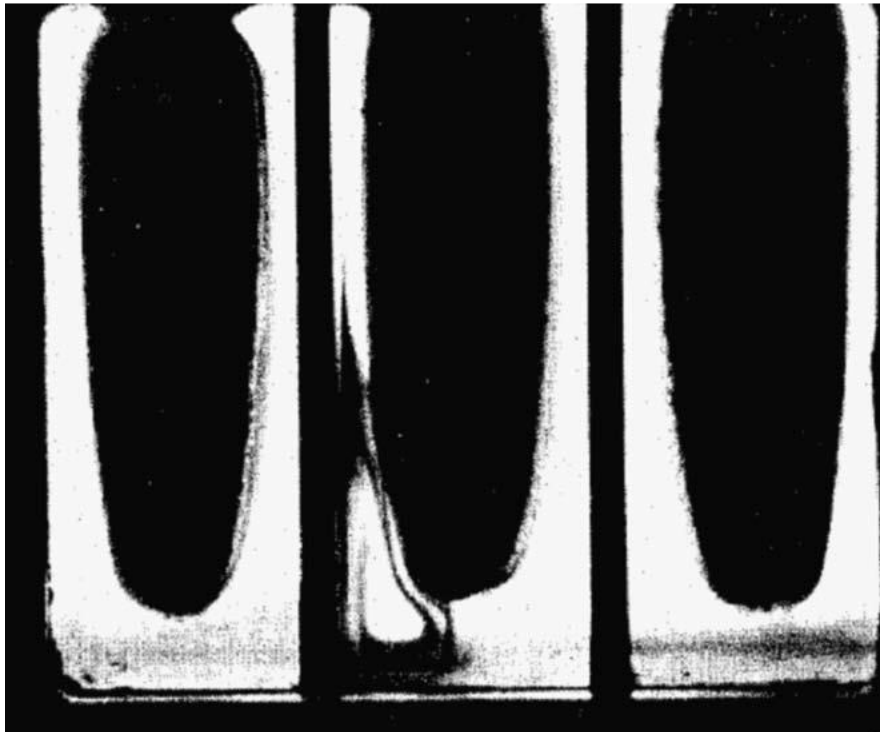


Figure 2.3: Flow visualization of natural convection-induced recirculatory vortex (Eftekhar *et al.*, 1984)

In summary, study of Eftekhar et al. (1984) provides valuable insights into optimizing thermal storage systems with PCM. By using an innovative approach of inducing natural

convection through fin arrangements, the research significantly advances the understanding of efficient heat transfer mechanisms in PCM-based thermal storage systems.

Scammel (2011) reported on his experimental studies that had many similarities with the experiments of Henze and Humphry (1981). A photograph of his experimental set-up showing five Plexiglas wall and one aluminum end that accommodates a heated element is shown in Figure 2.4.

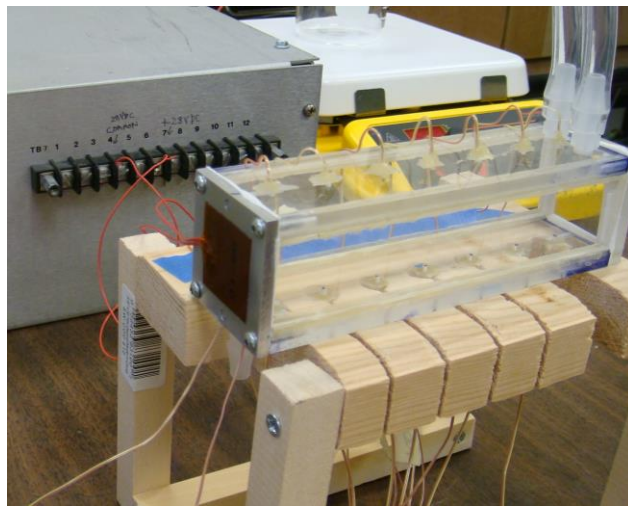


Figure 2.4: Experimental test-section of Scammel (2011)

Octadecane was the PCM utilized in this study. Moreover, some tests were conducted in presence of aluminum foams saturated with PCM. A series of photographs showing the progression of the LSI with and without aluminum foams are given in Figure 2.5.

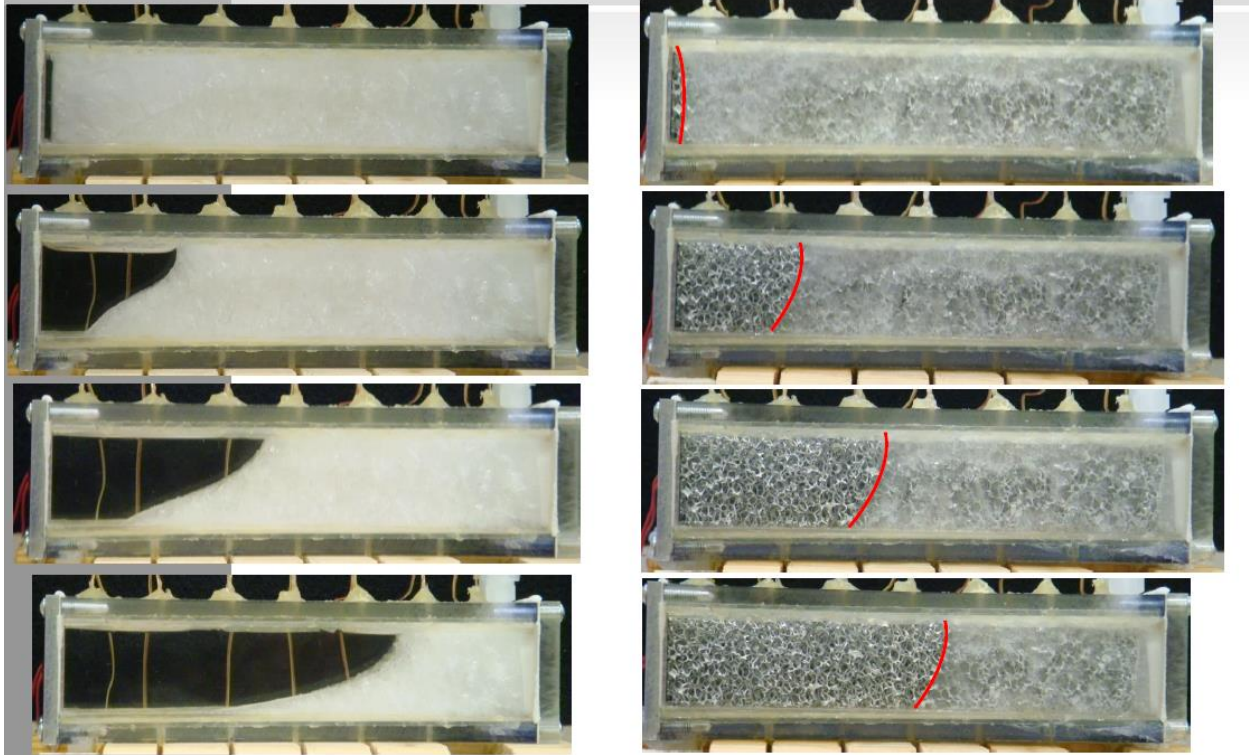


Figure 2.5: Time-varying progression of the LSI away from the vertical heated surface for case (a) without metal foam and (b) with metal foam (Scammel, 2011)

On the left side of Figure 2.5, progression of preferred melting at the top of the unit is clearly similar to those reported above by Henze and Humphrey (1981) for the case of unfinned system. The expanding liquid region is dominated by recirculating natural convection raising hot liquid that sinks along the colder curved LSI.

Having outlined the features of the relevant rectangular LHTES systems studied to date that have similarities to the current experimental cell, an overview of reported work on effects of mechanical vibrations on phase change systems follows.

2.2 Chronological Review of Prior Research on Mechanical Vibrations Affecting PCM

Research on phase change (transition) and LHTES systems has been expanding in recent years due to attractiveness of storing sizeable amount of thermal energy at a constant temperature in this mode of storage. However, very few research articles have focused on the influence of mechanical vibrations of performance of such systems. These studies are reviewed here.

Vadasz et al. (2016) aimed at investigating the effect of vibration on heat transfer and thus solidification rate of encapsulated phase change materials. Experiments were done with paraffin wax (RT35) stored inside hollow plastic spheres of 40 mm diameter with 1 mm wall thickness. The plastic sphere containing paraffin wax that was initially in a liquid state at a uniform temperature of 60 °C was then submerged into a thermal bath. This bath was held at a constant temperature of 15 °C which was approximately 20 °C below the mean solidification temperature of the wax. The spheres were then subjected to vertical vibrations with frequency of 10 to 300 Hz (Figure 2.6). The experimental results indicated a decrease in solidification time of 17% (or increase in heat transfer) during the solidification process with vibration when compared to the experiment process that does not contain vibration. This result was observed at an optimal vibration frequency of 100 Hz. The decay in the increased rate of solidification under vibration could also be seen in this study. The decay shown by the decrease in mass enhancement from 17% down to 2% suggests a possible oscillatory decay.

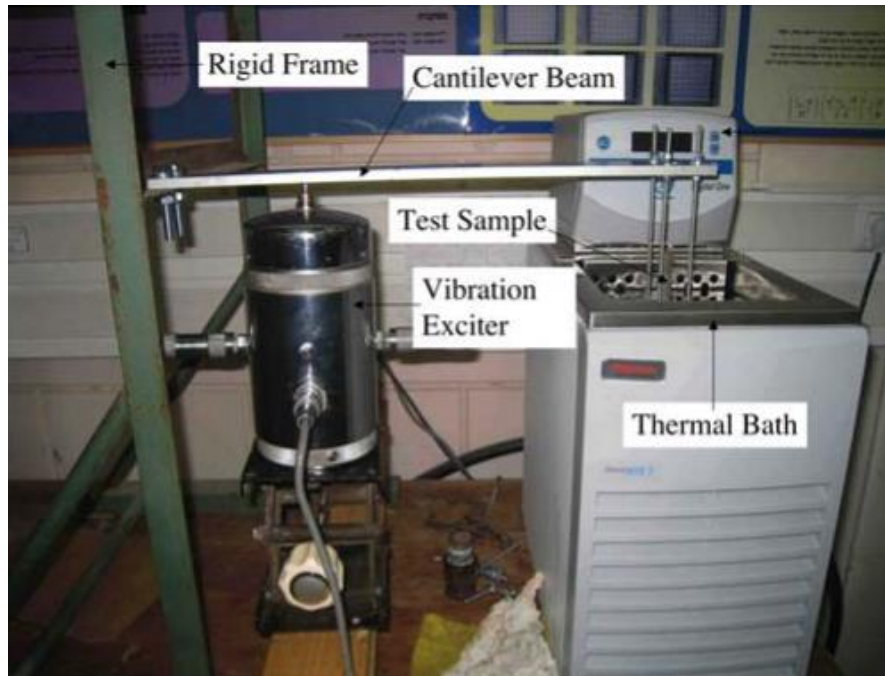


Figure 2.6 Experimental set-up of Vadasz et al. (2016) for solidification of paraffin stored within plastic spheres subjected to vertical vibrations

Joshy et al. (2020) reported findings of an experimental study that concentrated on effects of mechanical vibration on a PCM-based passive thermal management of a model battery of electric vehicles. They used Rubitherm 35HC PCM with a goal to maintain the battery temperature within the range of 25 °C to 40 °C. The simulated batteries are made of ten aluminum cylinders containing ceramic cartridge heaters at their cores that mimic the 2300 mAh 18650 lithium-ion batteries. A series of experimental tests were carried out collecting temperatures of individual cylinders to study the transient thermal field behavior of the battery pack under various discharge rates (i.e., 1–5C). The ranges of applied frequency and amplitude during the experiments (Figure 2.7) are 20–50 Hz and 30 mm/s to 50 mm/s, respectively, which are typically observed in plug-in hybrid electric vehicles (PHEV) on the road during normal operation. They found that temperature

at the battery surface exhibited a rising trend with increasing frequency and amplitude of vibration. However, the transient temperature variation pattern of batteries in the center of the battery pack was slightly different than the batteries in the corners.

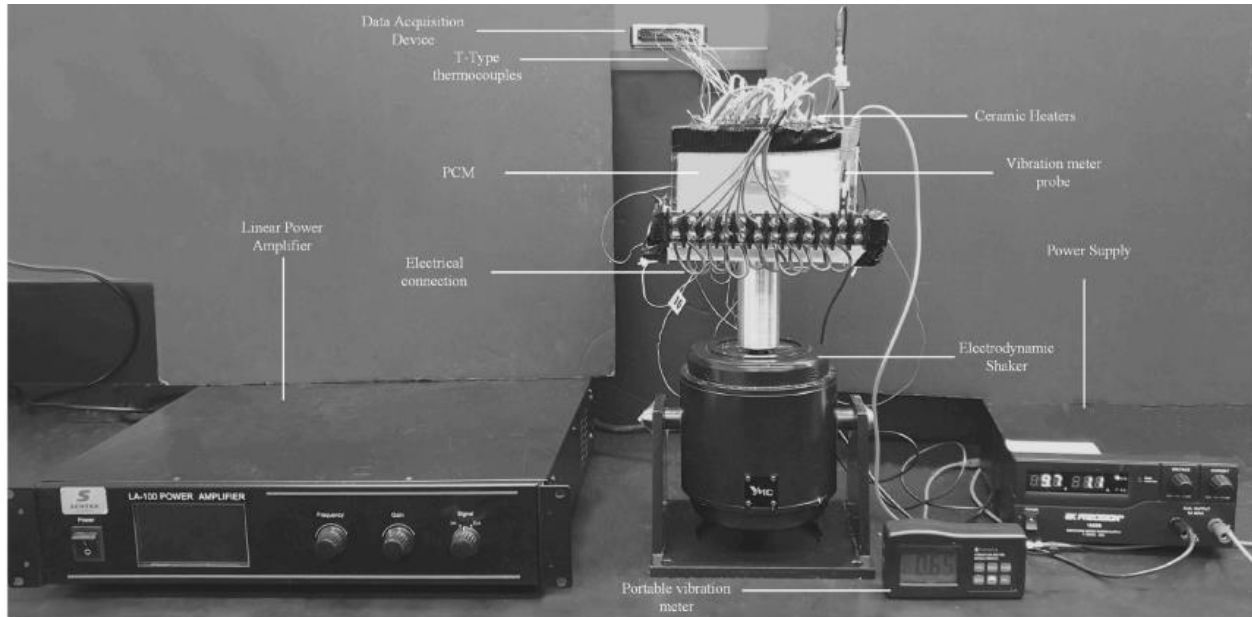


Figure 2.7: Components of the experimental set-up of Joshy et al. (2020)

Lee and Han (2022) reported findings of an experimental investigation (Figure 2.8) of the effect of random vibrations on the melting behavior of a phase change material and the thermal performance of a PCM-based heat sink. A random vibration from 2 to 16 g rms for the frequency range of 15 to 2000 Hz was applied to a rectangular enclosure which contained paraffin wax and the heat sink. A constant heat flux was imposed on the heat sink to melt the PCM. The time duration for the temperature of the heat sink to rise to a threshold value increased as the intensity of random vibration increased, 5.9 times longer under the vibration of 16 g rms than without vibration.

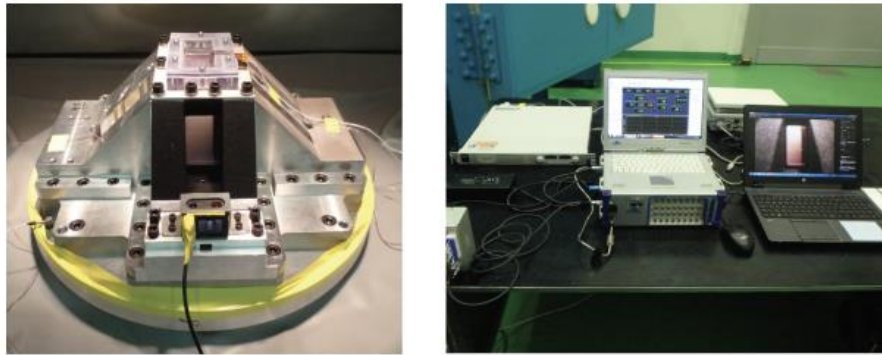
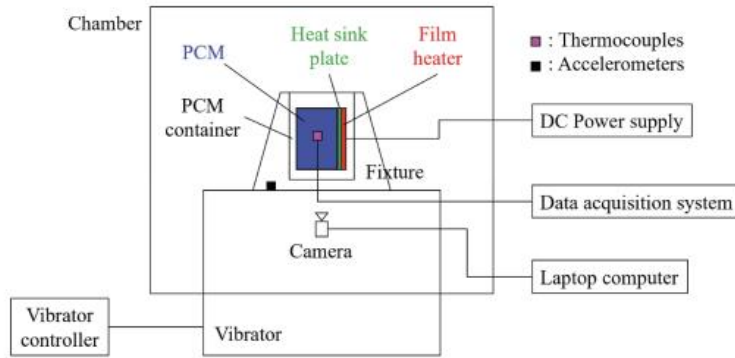


Figure 2.8: Experimental set-up of Lee and Han (2022)

From what has been discussed, Table 2.1 provides a quick overview of the operating conditions of experiments that have been performed on effects of mechanical vibrations on melting of PCM.

Table 2.1 Summary of the operating features of the mechanical vibration studies summarized above

| Authors | Experimental cell | PCM | Frequencies | Amplitude | Observations |
|----------------------|-------------------|-------------------------|-------------|-------------------|--|
| Vadasz et al. (2016) | Spherical | RT-35 | 10-300 Hz | 7.95 mm ± 0.15 mm | Faster solidification time |
| Joshya et al. (2020) | Rectangular | Rubitherm 35HC | 20-50Hz | 30 mm/s – 50 mm/s | Temperature increase on the surface with increase of frequency and amplitude |
| Lee and Han (2022) | Rectangular | Sigma-Aldrich ASTM D 87 | 15-2000Hz | 2G – 16G rms | Temperature of heat sink rise with increase of random vibration intensity |

2.3 Conclusions

Going over the small number of prior studies that involve mechanical vibrations in LHTES, presence of a conductive fin could enhance the rate of melting. Meanwhile, the orientation of the container will also affect the melting rate and the internal melting action for the PCM.

Meanwhile, the increase in amplitude or frequency could enhance the heat transfer process.

Chapter 3 Experimental Set-Up and Procedures

In this chapter, details related to experiment set-up, its design, fabrication and operation are outlined.

3.1 Experiment Apparatus

The PCM container is very similar to the one reported by Henze and Humphrey (1981). Two 2 inches by 4 inches aluminum plates with a thickness of 0.25 inches were machined with screw holes drilled from both sides. One of the metal plates that was designed to go to the top of the container accommodated two air ventilation holes that were drilled extra compared to the bottom plate that just have tiny holes for insertion of thermocouple. Five (5) holes on the top and nine (9) holes on the bottom aluminum plates were drilled. Holes were drilled on the plexiglass pieces which goes on 3 sides of the container test cells. Once these are done, the heater plate was machined out to a 2.5 inch * 2 inch * ¼ inch rectangular block, with the heater attached to one side and filled with thermal paste to enhance its thermal conductivity. With all the parts being machined, the first step is to glue the thermocouples into place.

The unit was placed on the lab table to give a near-perfect smooth surface so we can make sure our test beads on thermocouples are just sticking out the holes. Then, epoxy was applied to the other end of the thermocouple wires to keep it in place.

As thermocouples were being glued in place, gluing paste seal (Flex Glue Clear) that can sustain from -40 °C to 93 °C (-40 °F to 200 °F) was applied on the side of two metal plate. Upon connecting these aluminum plates with the Plexiglas, the same procedure was followed with the heater plate.

At this point, the container has 5 sides being glued together and left one end open for PCM filling purpose. But before this process can be applied, we tested our container with 80 °C hot water to check for any leakage. Once this step was done, the PCM and container were placed inside a vacuum oven (VWR 1430M) for initiation of the filling step. In this experiment, we chose 99% Octadecane (Aldrich Chemistry) as PCM and the technical information of this material is listed in Table 3.1.

Table 3.1: Thermophysical Properties of 99% Octadecane

| Properties | Value |
|--|-----------------------|
| Melting Point, (°C) | 28 |
| Density, ρ (kg m ⁻³) | 820.733 |
| Dynamic viscosity, μ (kg m ⁻¹ s ⁻¹) | 1.97×10^{-3} |
| Latent heat, L (kJ / kg) | 242.45 |
| Thermal conductivity, k (W m ⁻¹ K ⁻¹) | 0.151215 |
| Thermal expansion coefficient, β (K ⁻¹) | 8.9×10^{-4} |
| Specific heat, C _p (kJ / kg K ⁻¹) | 2.078 |

Once the PCM, container, beaker, funnel were all heated up, the PCM was slowly poured through the heated funnel next to the heater plate end of the test-section. Once the PCM was filled to the brim of our container, it was placed back into the vacuum oven and degassed to 0.25 atm, whereas the oven temperature was set to 45 °C to eliminate as much bubble or air inside the material as possible. This degassing process lasted for around 24 hours. After that, the oven was turned off for another 24 hours to allow the test-section to cool down and let the PCM to solidify. During the period, the PCM will shrink due to its change of density. The shrunk volume was replenished by adding liquid PCM on a few occasions.

With the container completely filled with solid PCM, the end plexiglass piece was attached. The whole container with then enclosed with styrofoam pads to give the container a better insulation during the experiments, whereas an insulated but removable styrofoam plate was placed on the front Plexiglas plate to allow visual access to the unit.

The various components for this experimental set-up are shown schematically in Figure 3.1, whereas a photograph is displayed below as Figure 3.2.

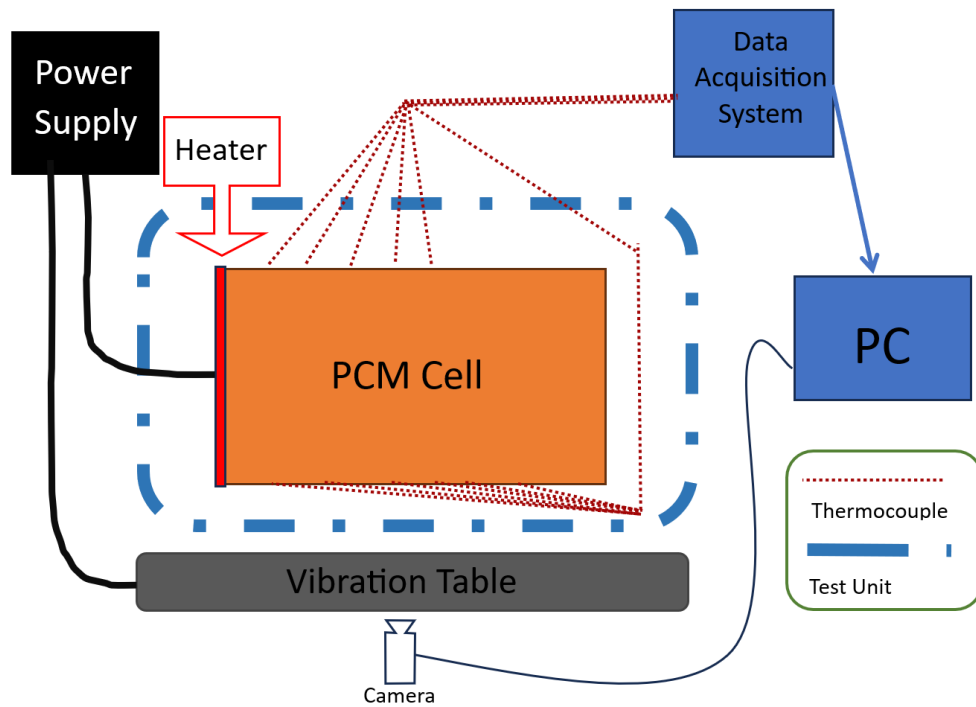


Figure 3.1: Schematic diagram of the experimental set-up



Figure 3.2: Photograph of the instrumented experimental set-up and various measurement components

3.2 Instrumentation

T-type thermocouples (Omega TT-40-SLE) were craft in-house and used for temperature measurement purposes in this experiment. Due to the limitation of our data acquisition system (National Instruments NI-9213), maximum of 16 thermocouples are available (channel 0-15). The configuration of thermocouples that were placed on the top and bottom aluminum plates are shown in Figure 3.3. There are a total of 14 thermocouple wires being glued on the aluminum plate, 5 of which (TC2-TC6) are placed on the top and 9 others (TC7-15) on the bottom plate. One other thermocouple (TC0) measured the ambient air temperature in the laboratory and last one (TC1) was glued to the heater plate to measure the temperature of the heater plate.

Figure 3.3: Thermocouple Locations (note matching of the vertical positions of some thermocouple pairs, i.e., 2 & 7, 4 & 9, 5 & 11)

A variable transformer (Superior type: 3PN116C) was used as our controllable power supply to power the Omega flex heater (KHA-105/10-P). A multimeter (HP 3468A multimeter) was used to measure the AC voltage and a clamp multimeter (Klein Tools CL390) was utilized to measure the current flow through the wire, so that one can determine the power which the heater is drawing. Our data acquisition chassis was the National Instruments NI-9014 operated by the NI LabVIEW 2019 (32-bit) software and the camera for storing video information was a Logitech 1080P webcam.

The vibration tests were conducted via a number of instruments, i.e. a Vertical Shaker (Ling Dynamic System LTD (LDS), model number V465), a Power Amplifier (LDS PA 500L) and a Dynamic Signal Analyzer (Hewlett Packard 35665A) that were put together as shown in Figure 3.4



Figure 3.4: Vibration Table Set-Up

3.3 Experimental Procedure

The experiments were initiated by setting the power manually to 110 V from a voltage transformer, while starting the recording software and a clock on the computer. At every 2.5 minutes, the front foam pad cover was removed to allow visual access to the test-section. The power was turned off at 30 minutes time instant, however recording of temperature data was continued for another 5 minutes.

This process was repeated for the container under non-vibration tests at different inclination angles. All data and pictures were collected for further analysis.

For the mechanical vibration tests, the desired vibration frequency can be entered from the instrument but not the acceleration. Instead, what we can input is level, but that input level will not fully represent final outcome, so a laser measuring device was introduced to measure the actual vibrated level on the testing cell, then with a number of calculations being performed, the acceleration can be determined that way. The equation and example calculations are listed below, the Y-value is the actual signal sensor by the equipment where the displacement was measured by the laser.

Assuming a harmonic sine wave vibration, the displacement (x) is:

$$x = a \sin\omega t \quad (3.1)$$

where the angular velocity is related to frequency (f) via:

$$\omega = 2\pi f \quad (3.2)$$

Upon differentiating Equation (3.1) twice, we obtain:

$$Acceleration (G) = a(4\pi^2f^2) \quad (3.3)$$

In order to know the actual displacement, one needs the Y-value (mV rms) from the dynamic signal analyzer, and the displacement measurement ($\mu\text{m}/\text{V}$)

$$Displacement(mm) = Y(mV \text{ rms}) * Measurement (\mu\text{m}/\text{V}) \quad (3.4)$$

Equation 3.4 gives the peak-to-peak value between the top and bottom of the shaker, so to get the amplitude (mm), equation 3.5 is needed:

$$Amplitude (mm) = \frac{Displacement}{2} \quad (3.5)$$

Upon knowing the amplitude and frequency, the acceleration (G) will follow using equation 3.6:

$$Acceleration (G) = \frac{Amplitude (mm)}{1000 \frac{mm}{m}} * \frac{4\pi^2 f^2}{9.8} \quad (3.6)$$

With the equation 3.6, the proper G -level can be found with the input frequency and readout from the instrument. Table 3.3 gives the sample data of how the G -level was been determined for this experiment.

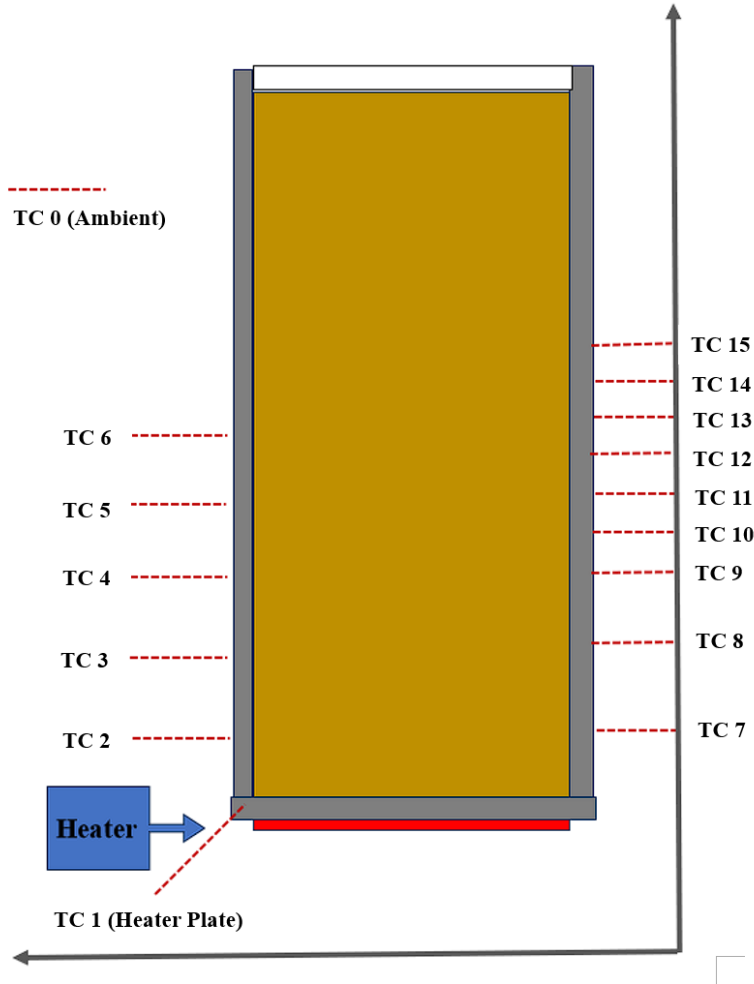


Table 3.3: Sample calculation of getting the acceleration

| | Read of Instrument | | | | Calculation | | |
|-----------------|--------------------|---------------|-----------------|--------------|---------------|-----------------|--------------|
| Runs | Input(mVrms) | Frequency(Hz) | Runs | Input(mVrms) | Frequency(Hz) | Runs | Input(mVrms) |
| 50 Hz 1G | 175 | 50 | 50 Hz 1G | 175 | 50 | 50 Hz 1G | 175 |
| 100 Hz 1G | 270 | 100 | 100 Hz 1G | 270 | 100 | 100 Hz 1G | 270 |

Chapter 4 Experimental Results

Detailed findings of the experimental studies conducted in the course of this investigation will be presented and discussed in this Chapter.

Two sets of experiments corresponding to cases of (i) no vibrations and (ii) vibrations were conducted. The results for the cases with no mechanical vibrations are presented in section 4.1 for the inclinations angles of 90, 60, 45, 30 and 0 degrees. The test cases for experiments under mechanical vibrations are discussed in section 4.2. For all cases reported in this study, the power levels were maintained nearly constant. The pertinent power levels delivered to the system are discussed in section 4.5.

4.1 Experimental Data for Cases with No Vibration

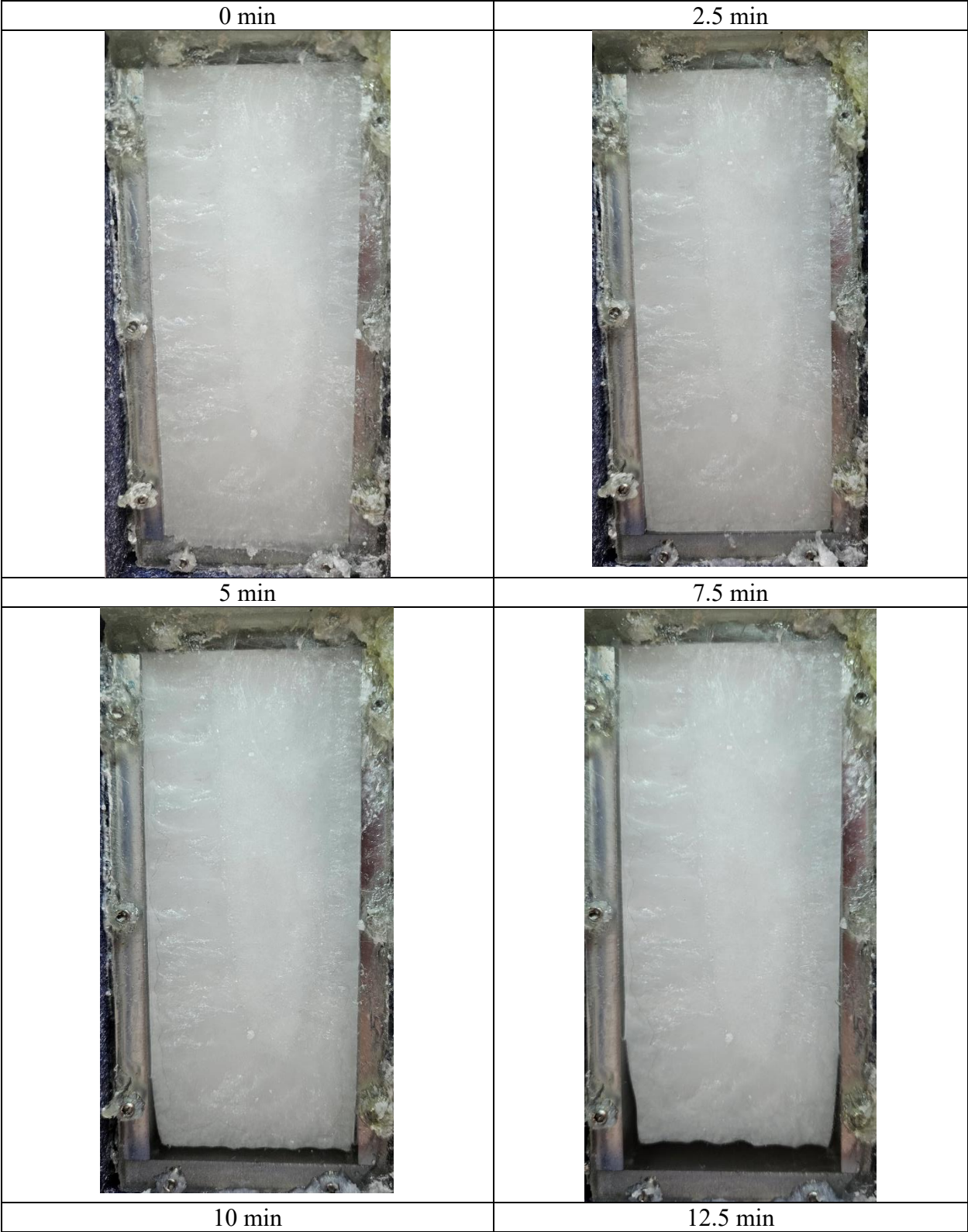
In this section, melting of the PCM within the test cell for inclinations angles of 90, 60, 45, 30 and 0 degrees will be discussed. For the 90-degree case, the heated plate is the lowest horizontal plane of the test cell and the hot molten PCM can easily rise along the two heated vertical aluminum plates. This configuration has great similarity with previous study of Eftekhar et al. (1984). At the other extreme, for the 0 degree case, the heated plate is the vertical plane on the left, a configuration that has great similarity with findings of Henze and Humphrey (1981).

4.1.1 Results for the Orientation Angle of 90°

Corresponding to melting without vibration for the orientation angle of 90°, instantaneous photographs of the front observation window of the experimental set-up obtained at various time instants of 0, 2.5, 5, 7.5, 10, 12.5, 15, 17.5, 20, 22.5, 25, 27.5 and 30 minutes are shown in

Figures 4.1 and 4.2. The temporal variations of temperatures corresponding to case of Figure 4.1 are presented in Figure 4.3, where temperatures registering the ambient condition, heated surface and the two heated plates (left and right in Figure 4.1) are designated in different colors. The lowest and highest registered temperatures correspond to the lab environment and thermocouple embedded in the heated aluminum plate, respectively. The melting temperature of the PCM is also drawn as a dashed line. The heat input into the unit was stopped at the time instant of 30 minutes, however the temperature readings are shown up to the 32 minutes time instant. Formation of a wavy LSI at the time instant of 5 minutes and its persistence to the 10-minute time instant are clearly observed. In this time period, a thermally-unstable layer separating the hotter heater plate at the bottom and colder solid PCM above the liquid PCM is created, thus promoting buoyancy-driven convection. These natural convection currents, in turn create the wavy interface of the thawing PCM.

Due to the geometrical symmetry of the system in relation to the gravitational acceleration, the melting patterns should also be symmetric and the temperatures recorded at the same heights should be identical. However, the melting pattern inside the cell was extremely unsymmetric. The causes of this observation could be the presence of trapped air bubbles, and leakage of the liquid PCM out of the unit. All these could cause the unsymmetric melting and the thermocouple readings also proved the lack of symmetry. For instance, thermocouples 2 and 7 that are at the same vertical levels in this configuration pointing directly at each other at same height, were exhibiting more than 9 degrees Celsius difference. This suggests that the left and right side of the PCM are experiencing marked temperature difference which suggests that there will be noticeable difference on the melting pattern.





15 min



17.5 min



20 min



22.5 min



25 min



27.5 min



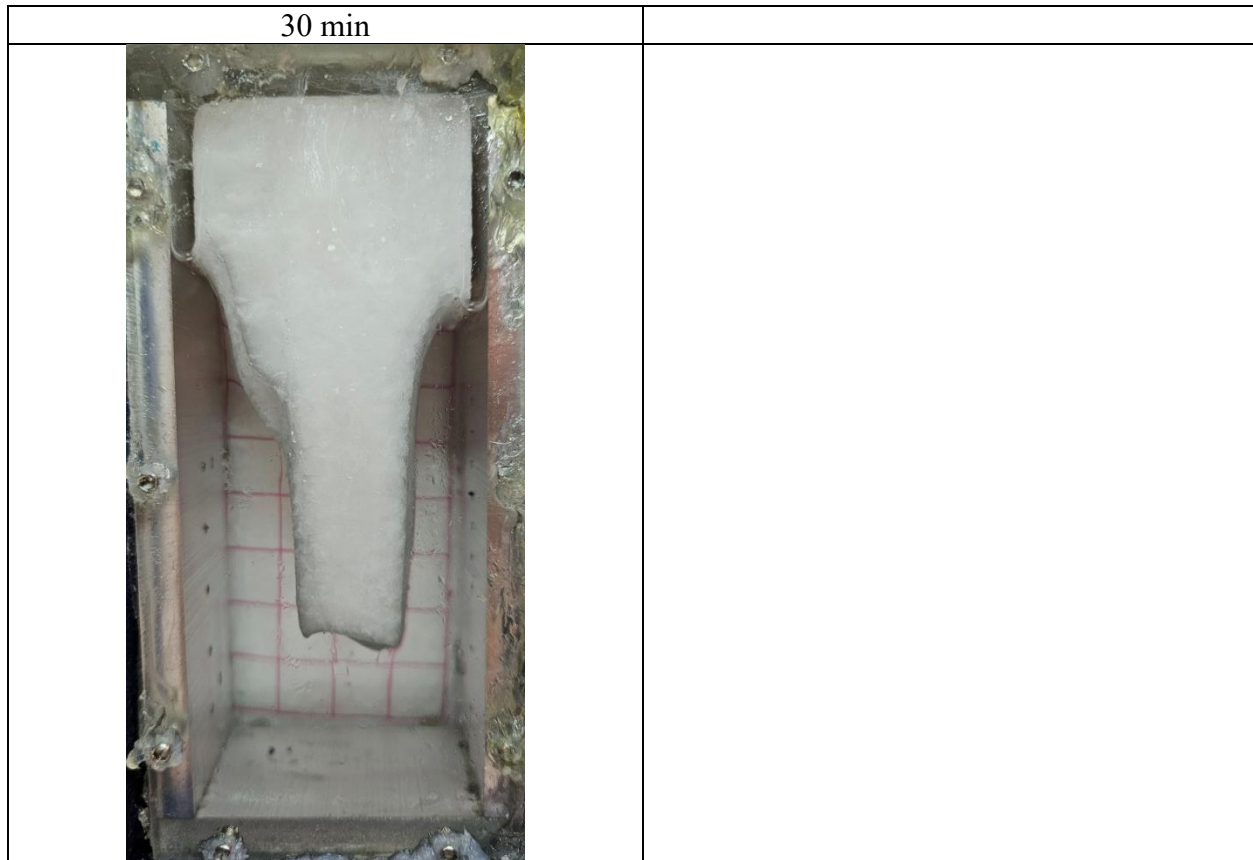


Figure 4.1 Instantaneous progression of the liquid-solid interface on the front observation window of the set-up during melting without vibration for the inclination angle of 90 degrees (horizontally-oriented heated plate at the bottom)

A slanted view of the experimental set-up is shown as Figure 4.2, which proves that contrary to the assumed two-dimensional melting in such a system, there is marked 3-dimensional thawing inside the test cell. In effect, the uneven melting can not be captured by the images of the observation window of Figure 4.1.

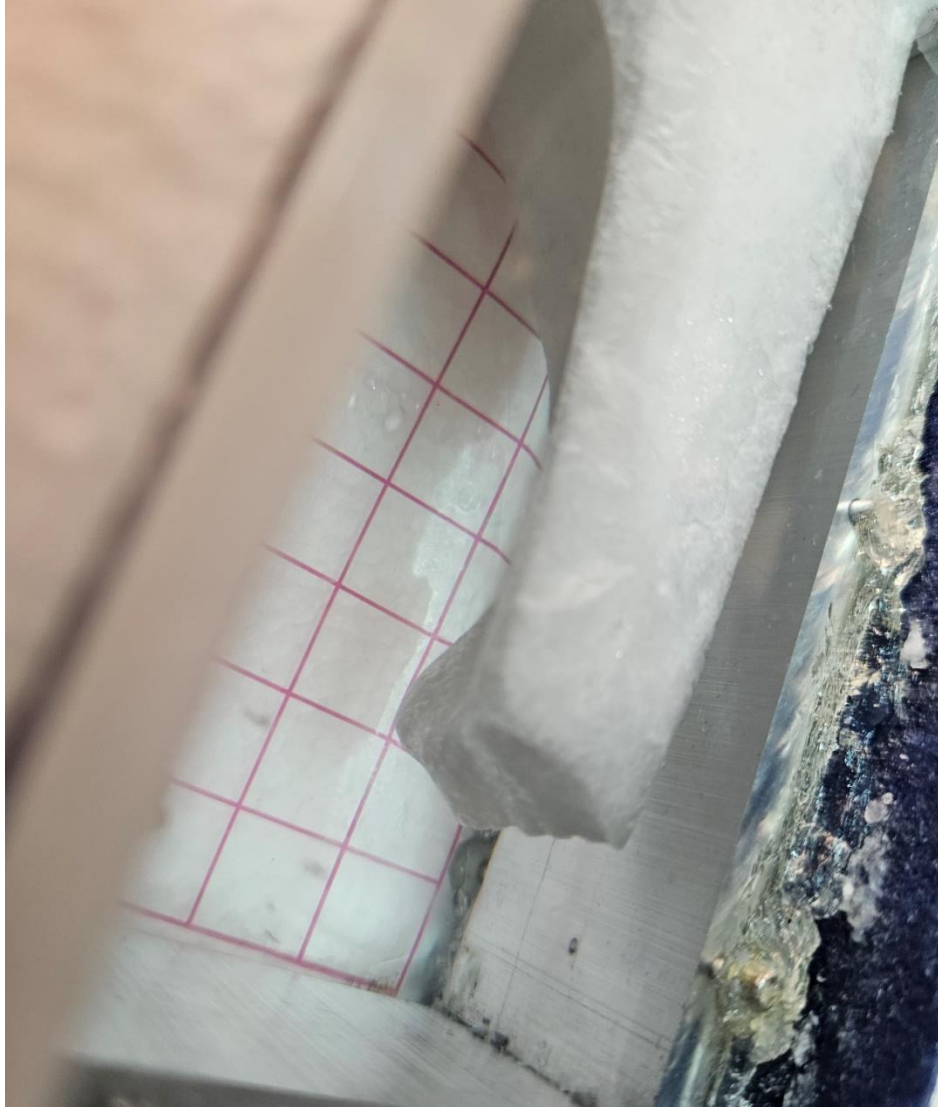


Figure 4.2: Slanted View for the Evidence of 3-Dimensional Melting ($t > 30$ minutes)

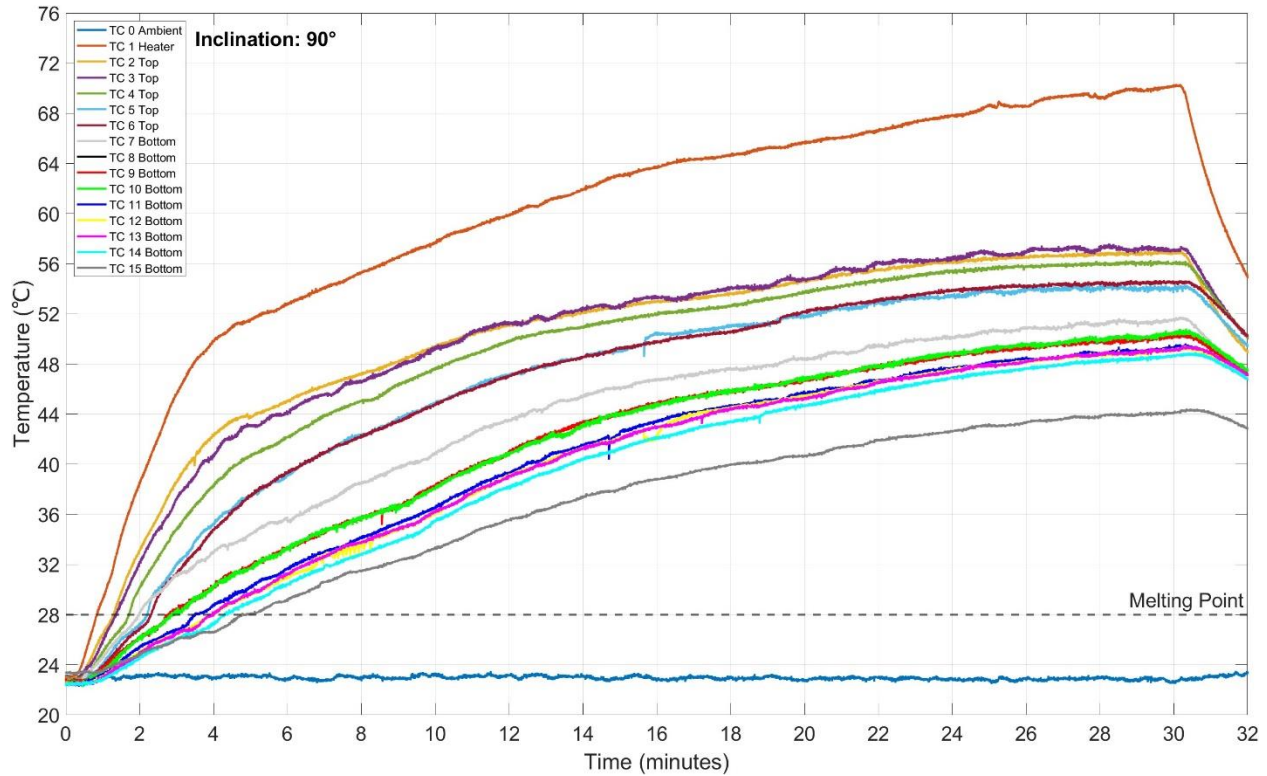


Figure 4.3: Temperature variations with time during Melting Without Vibration for the inclination angle of 90 degrees (horizontally-oriented heated plate at the bottom)

4.1.2 Results for the Orientation Angle of 60°

The system described in the previous section was then rotated clockwise by 30 degrees. Instantaneous photographs of the front observation window of the experimental set-up obtained at 2.5 minutes time intervals from start of heating and ending at the 30 minutes time instant for the no vibration case with inclination angle of 60 degrees are shown in Figure 4.4. Temporal variations of temperatures corresponding to case of Figure 4.4 are presented in Figure 4.5.

Banding of the thermocouples installed on the two aluminum planes (TCs 2-6 and TCs 7-15) are clearly observed in Figure 4.5 when compared to Figure 4.3. Arguing that nearly identical heat conduction from the heated plate enters each of the aluminum plates, this banding indicates

more marked influence of natural convection on the aluminum plate that is downstream of the rising hot liquid emerging from the heated plate.

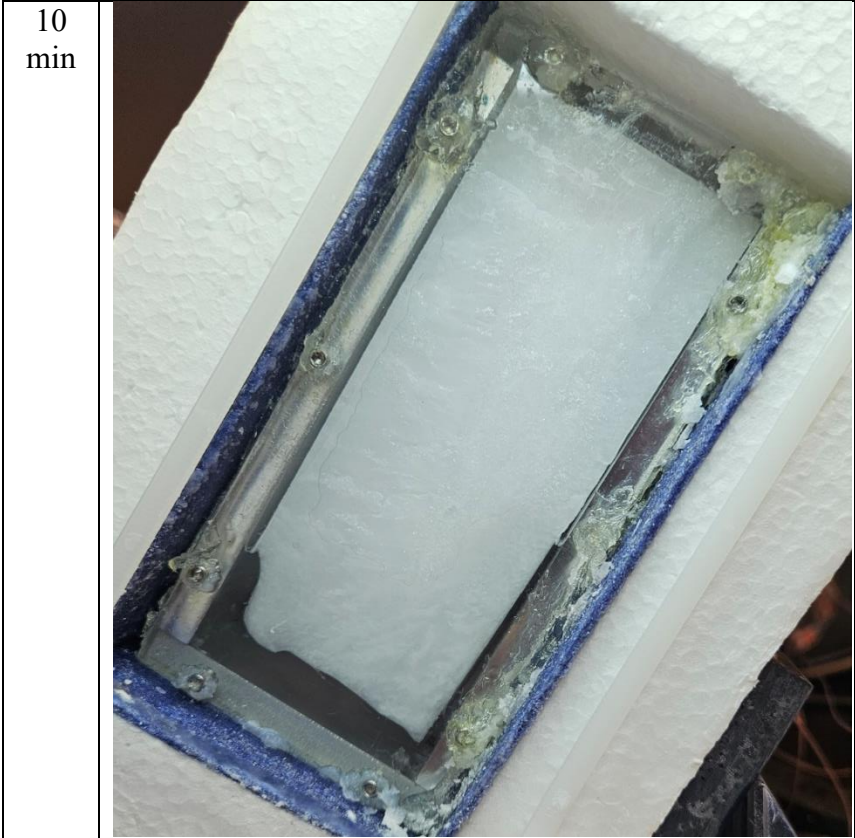




2.5
min



5
min







| | |
|---------------------|--|
| <p>12.5 min</p> |  A photograph showing a rectangular assembly within a white foam container. The assembly consists of a central white rectangular block held between two metal plates. The metal plates are secured by screws. A blue material is visible along the edges of the assembly. The assembly is surrounded by a white foam insulation layer. |
| <p>15 min</p> |  A photograph showing the same rectangular assembly as in the 12.5 min image. The assembly is identical, consisting of a central white rectangular block held between two metal plates, secured by screws, and surrounded by a blue material and white foam insulation. |

17.5
min



20
min



| | |
|---------------------|---|
| <p>22.5 min</p> |  A photograph showing a mold assembly. A white, rectangular, porous material is being formed within a blue frame. The material is partially solidified and has a slightly irregular, porous appearance. The frame is mounted on a white, textured surface. The assembly is held together by several screws. |
| <p>25 min</p> |  A photograph showing the same mold assembly as in the previous image, but at a later time. The white, porous material has become more solid and has a more uniform, rectangular shape. The porous appearance is less pronounced, and the material appears more like a solid block. The frame and mounting are the same as in the previous image. |

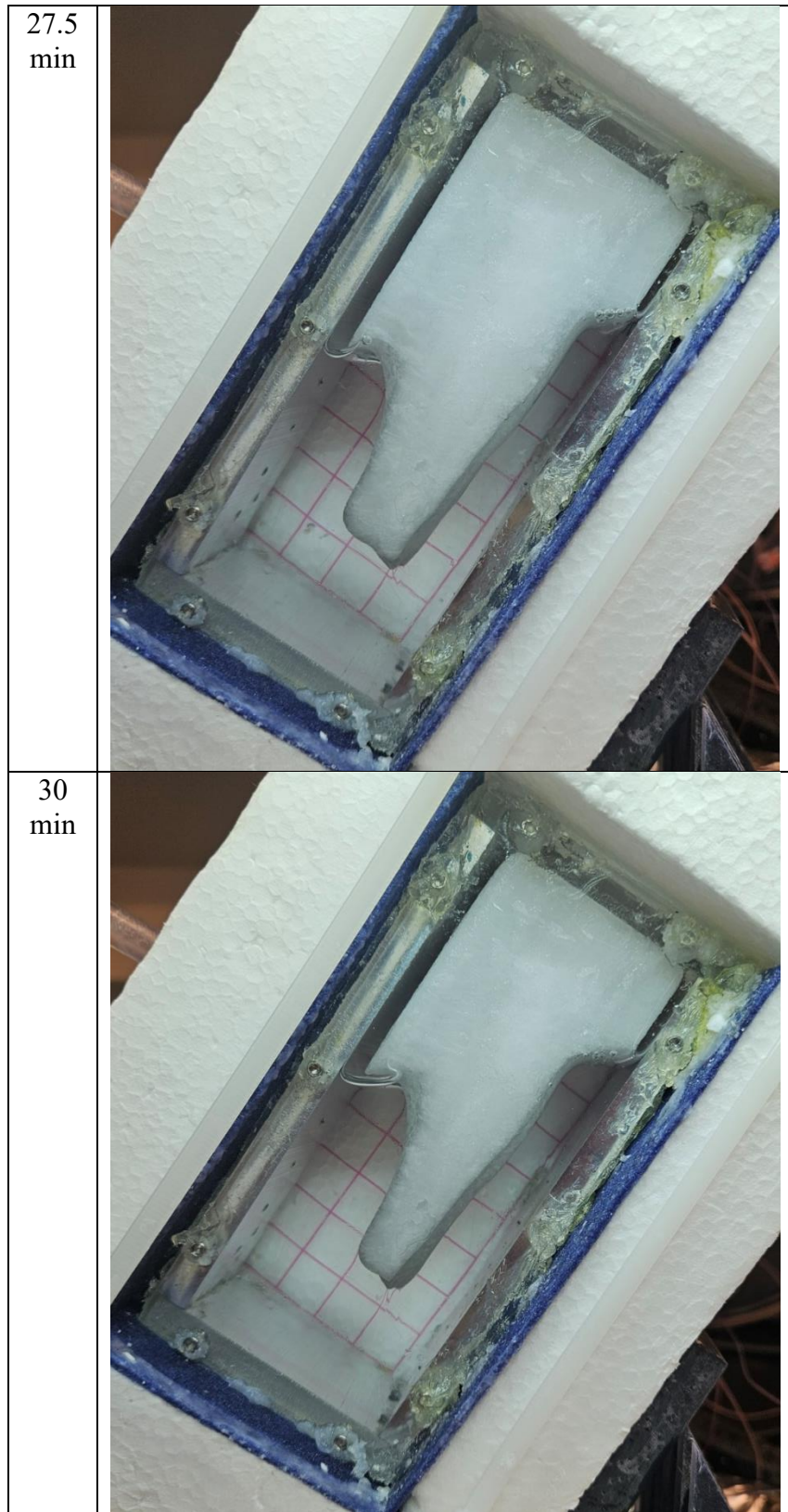


Figure 4.4: Instantaneous progression of the liquid-solid interface on the front observation window of the set-up during Melting Without Vibration for the inclination angle of 60 degrees

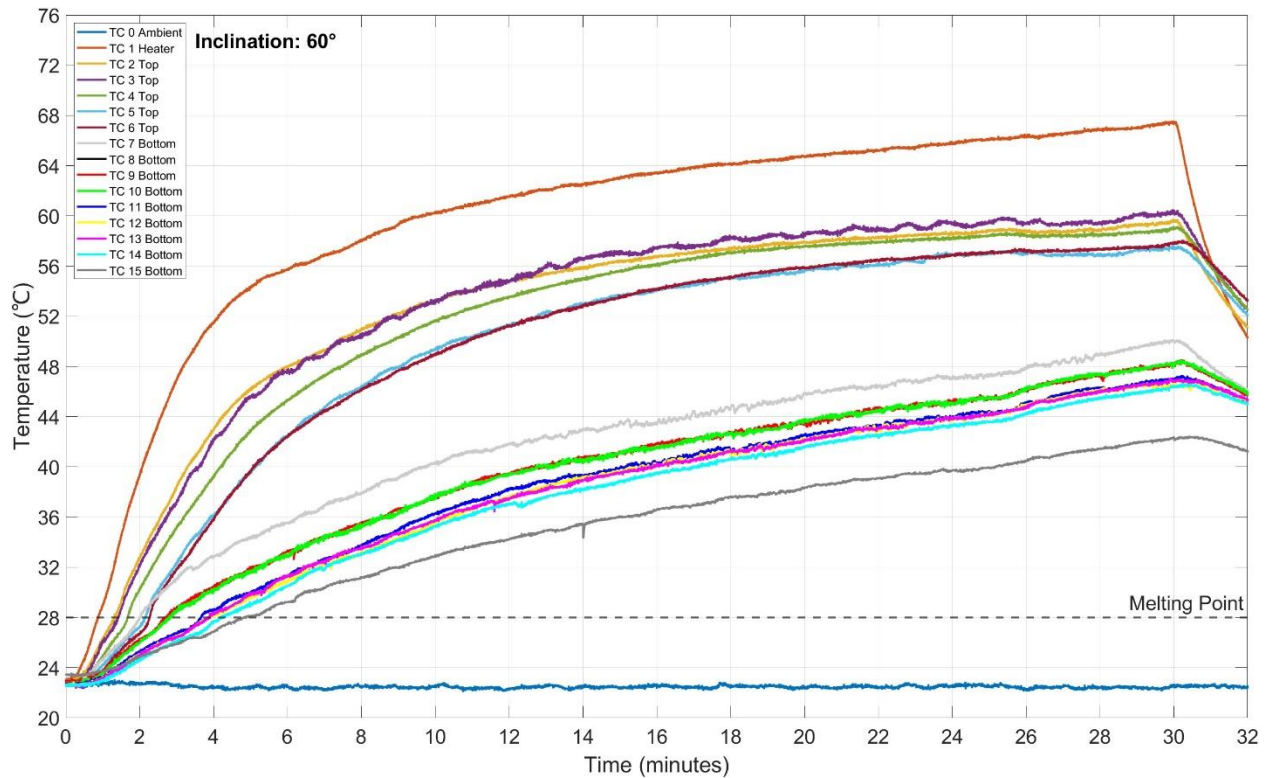


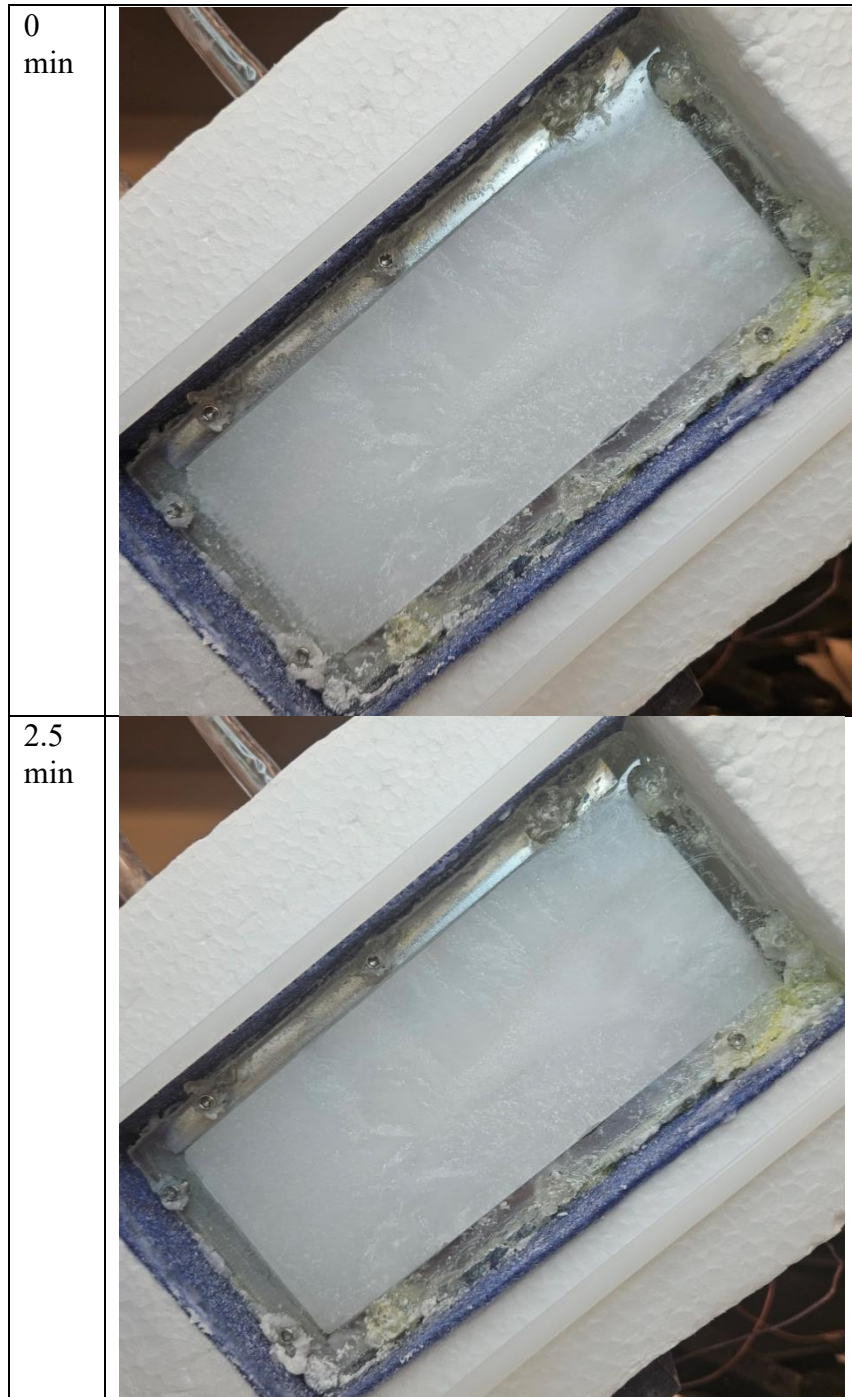
Figure 4.5: Temperature variations with time during Melting Without Vibration for the inclination angle of 60 degrees

4.1.3 Results for the Orientation Angle of 45°

Instantaneous photographs of the front observation window of the experimental set-up obtained at 2.5 minutes intervals from start of heating and ending at the 30 minutes time instant for the no vibration case with inclination angle of 45 degrees are shown in Figure 4.6. The corresponding temporal variations of temperatures to case of Figure 4.6 are presented in Figure 4.7.

Further banding of the thermocouples installed on the two-aluminum heat conducting planes are more clearly observed in Figure 4.7 when compared to Figures 4.3 and 4.5.

A number of oscillations was captured by thermocouples which suggests that there might be evolving fluid cells moving on the both aluminum plate surfaces.





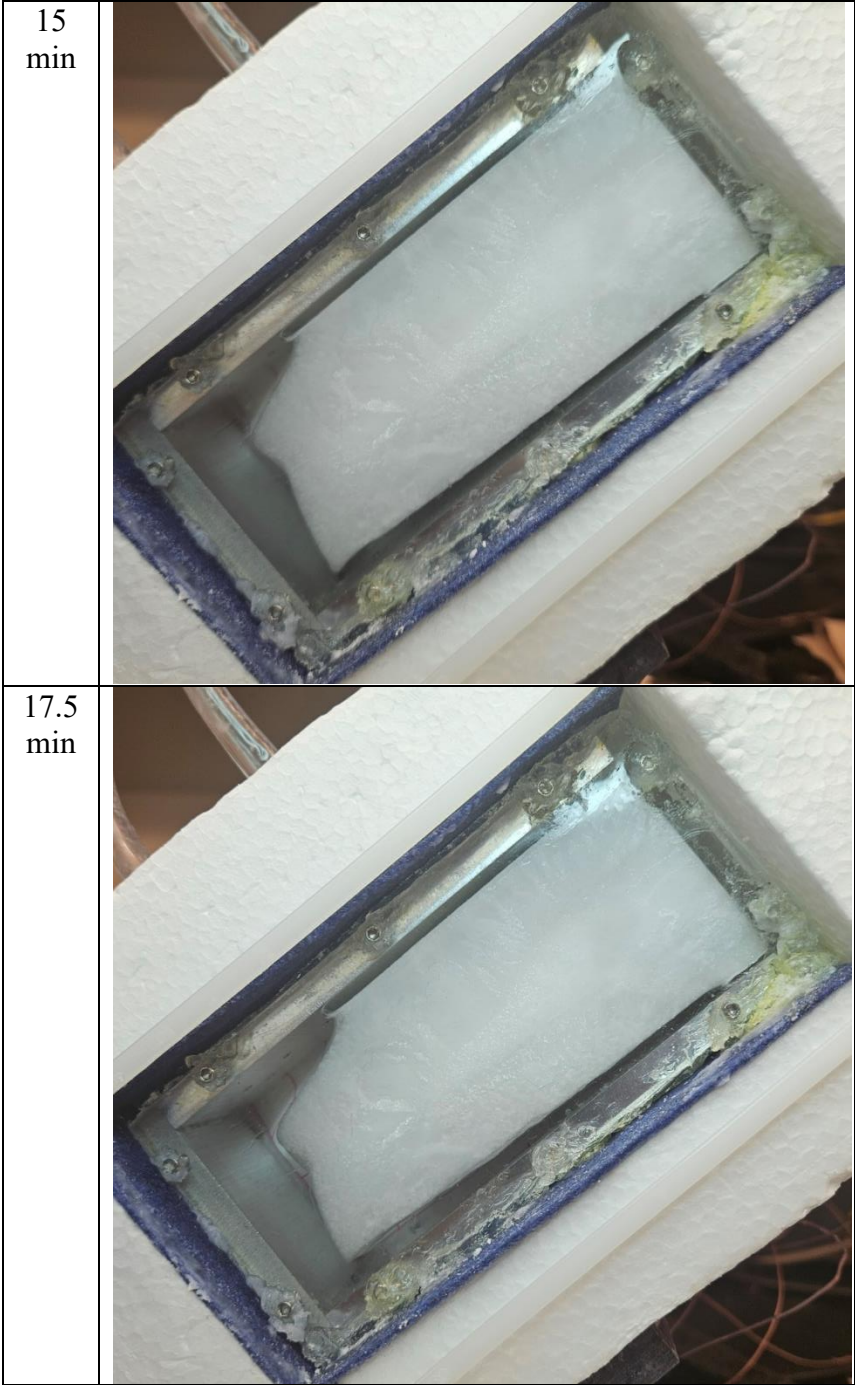
5
min

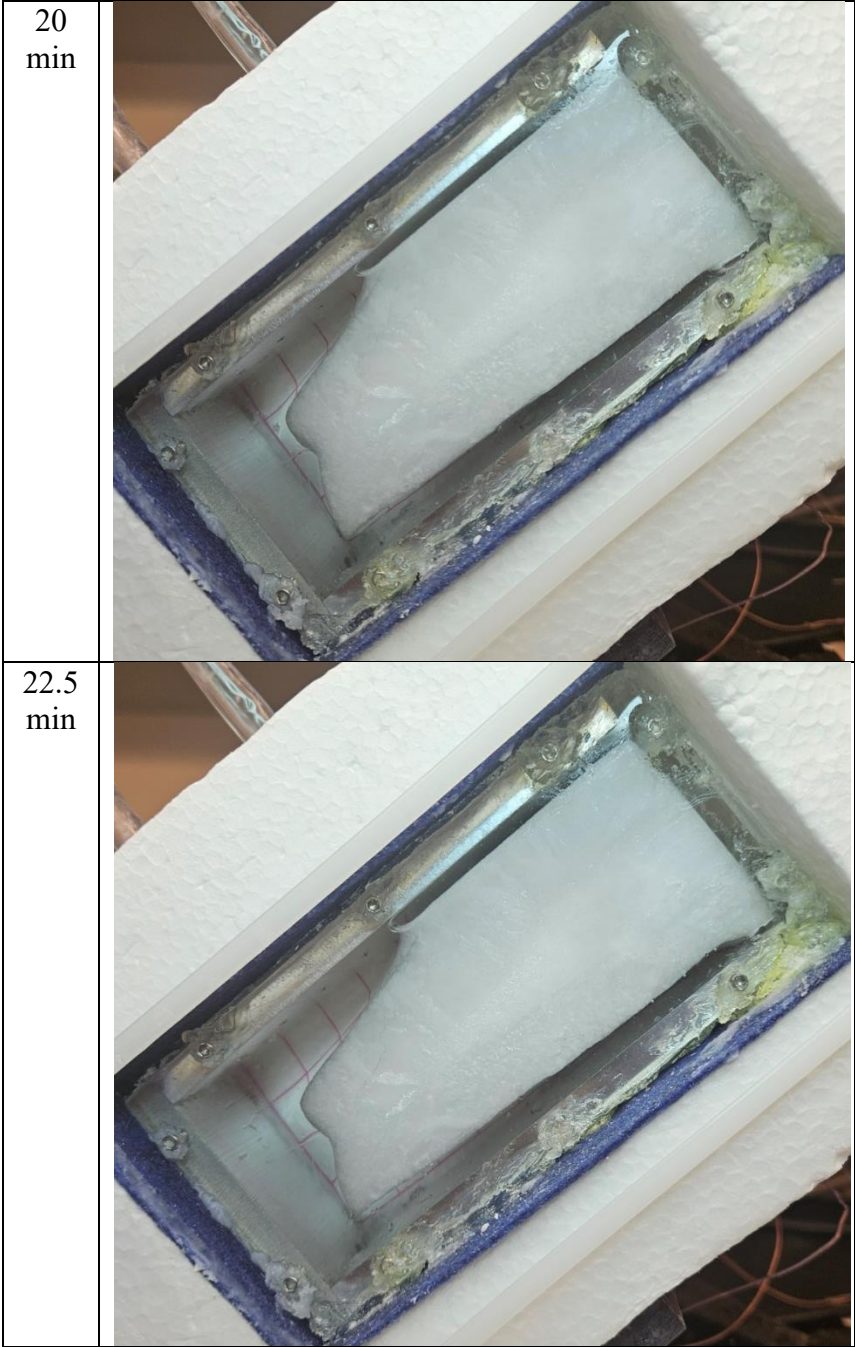


7.5
min



| | |
|---------------------|---|
| <p>10 min</p> |  |
| <p>12.5 min</p> |  |





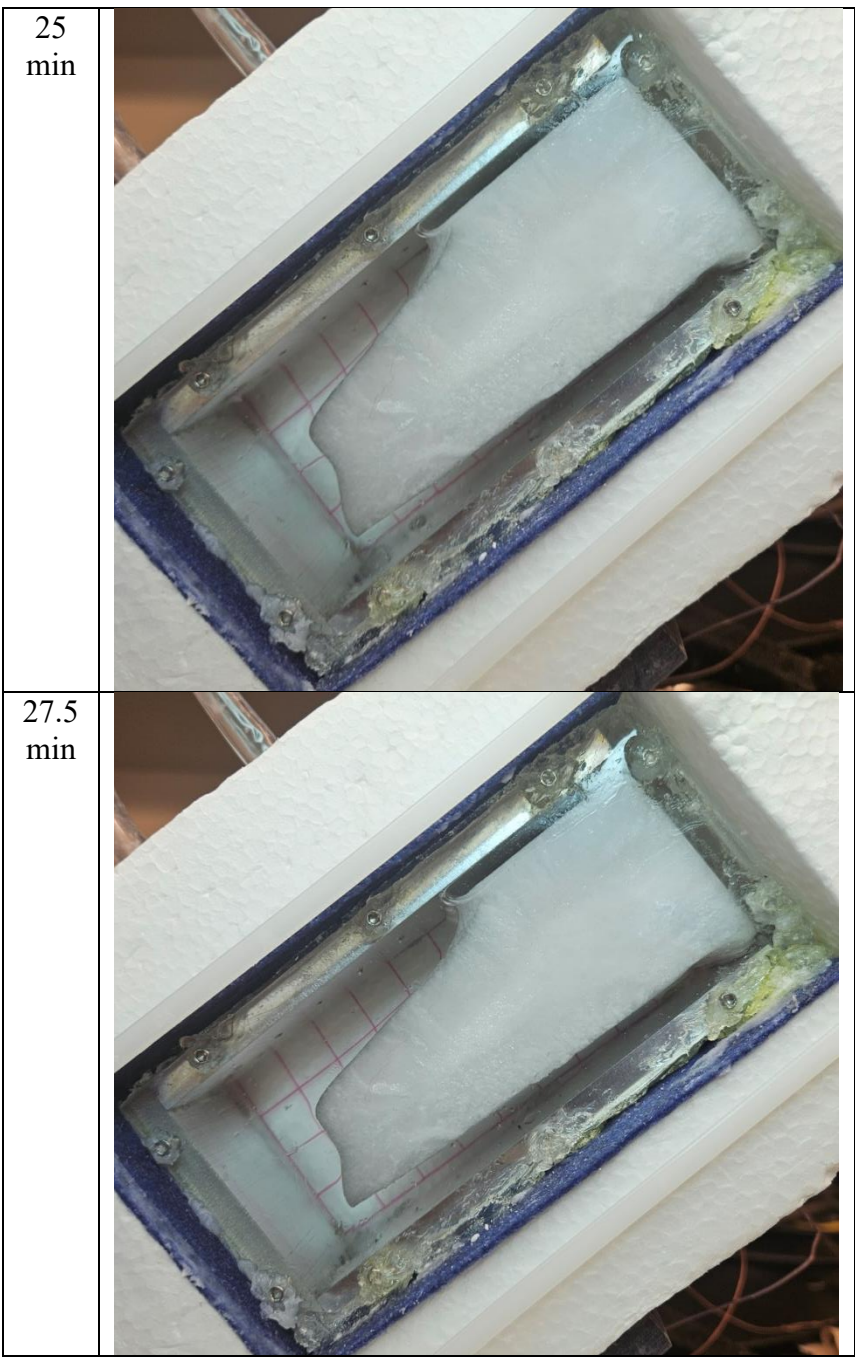




Figure 4.6: Instantaneous progression of the liquid-solid interface on the front observation window of the set-up during Melting Without Vibration for the inclination angle of 45 degrees

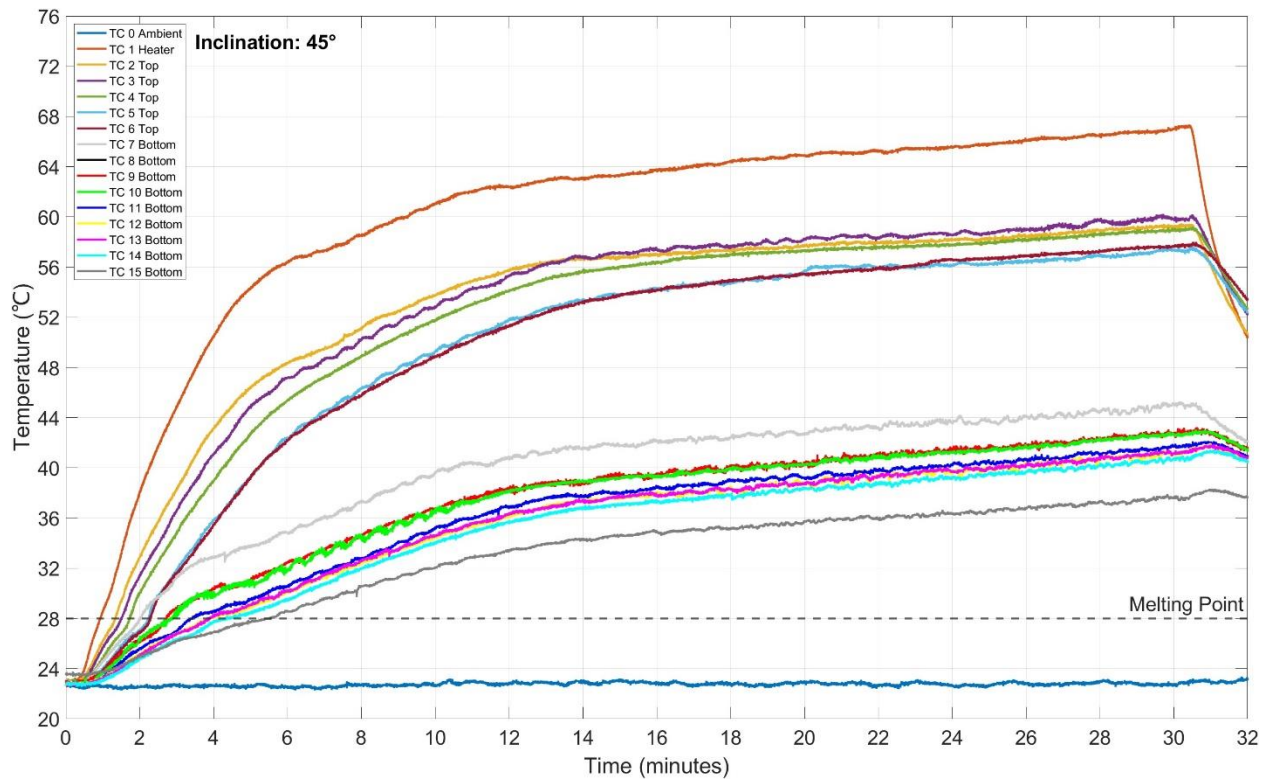

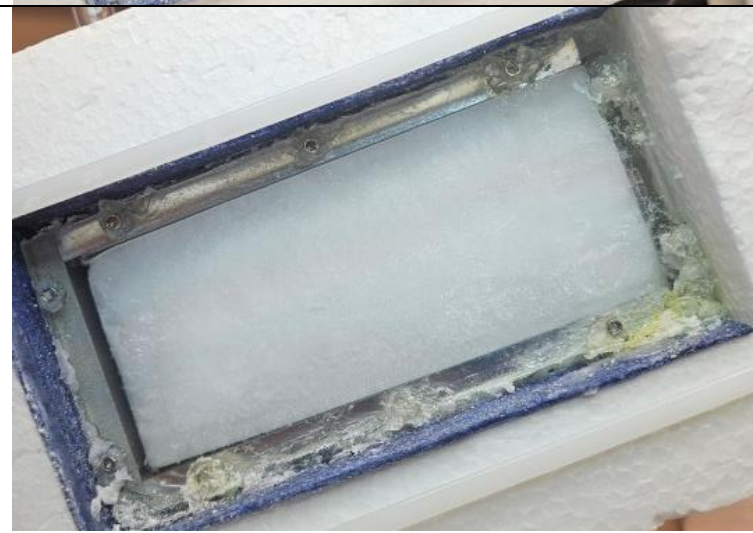






Figure 4.7: Temperature variations with time during Melting Without Vibration for the inclination angle of 45 degrees



4.1.4 Results for the Orientation Angle of 30°



Instantaneous photographs of the front observation window of the experimental set-up obtained at 2.5 minutes intervals from start of heating and ending at the 30 minutes time instant for the no vibration case with inclination angle of 30 degrees are shown in Figure 4.8. The corresponding temporal variations of temperatures to case of Figure 4.8 are presented in Figure 4.9. Whereas the banding of temperature readings is maintained, the thermocouple oscillations exhibit longer periods.



| | |
|------------|--|
| 2.5 min |  |
| 5 min |  |
| 7.5 min |  |

| | |
|-------------|--|
| 10 min |  |
| 12.5 min |  |
| 15 min |  |

| | |
|-------------|---|
| 17.5 min |  |
| 20 min |  |

| | |
|-------------|---|
| 22.5 min |  |
| 25 min |  |

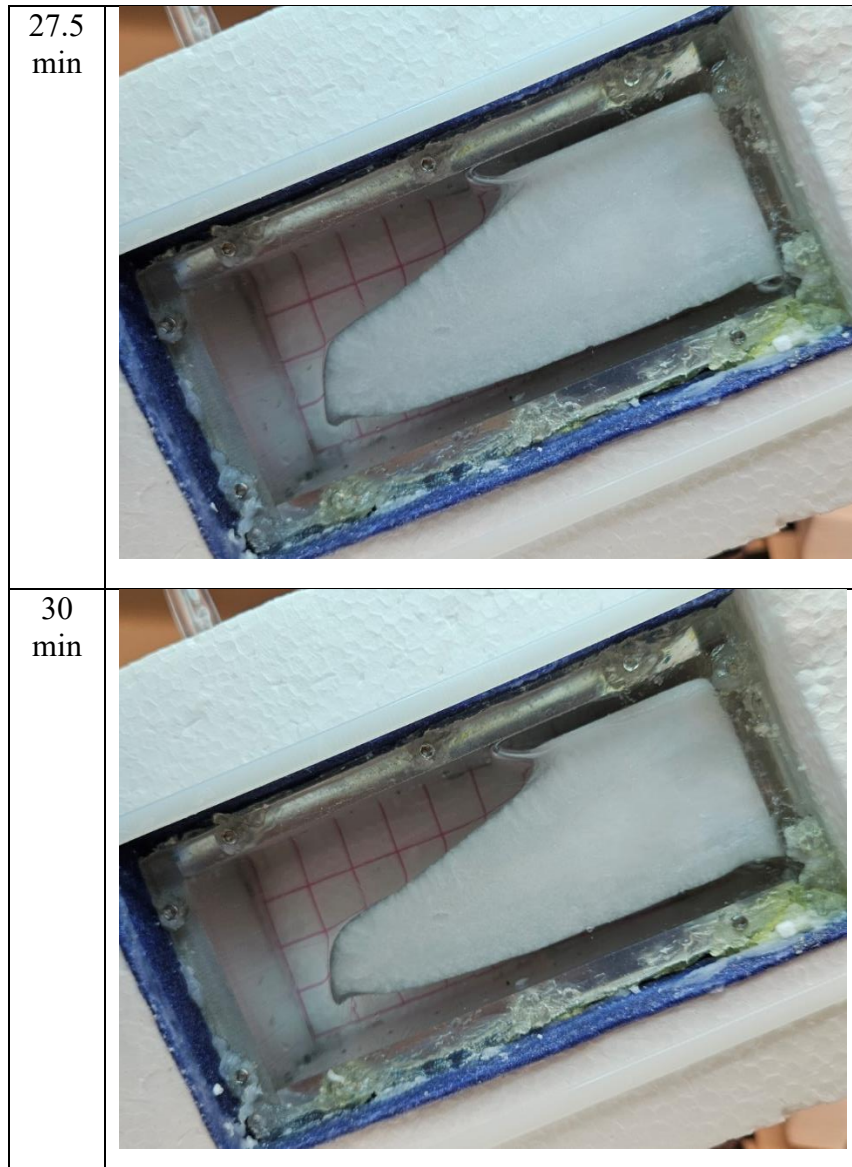


Figure 4.8: Instantaneous progression of the liquid-solid interface on the front observation window of the set-up during Melting Without Vibration for the inclination angle of 30 degrees

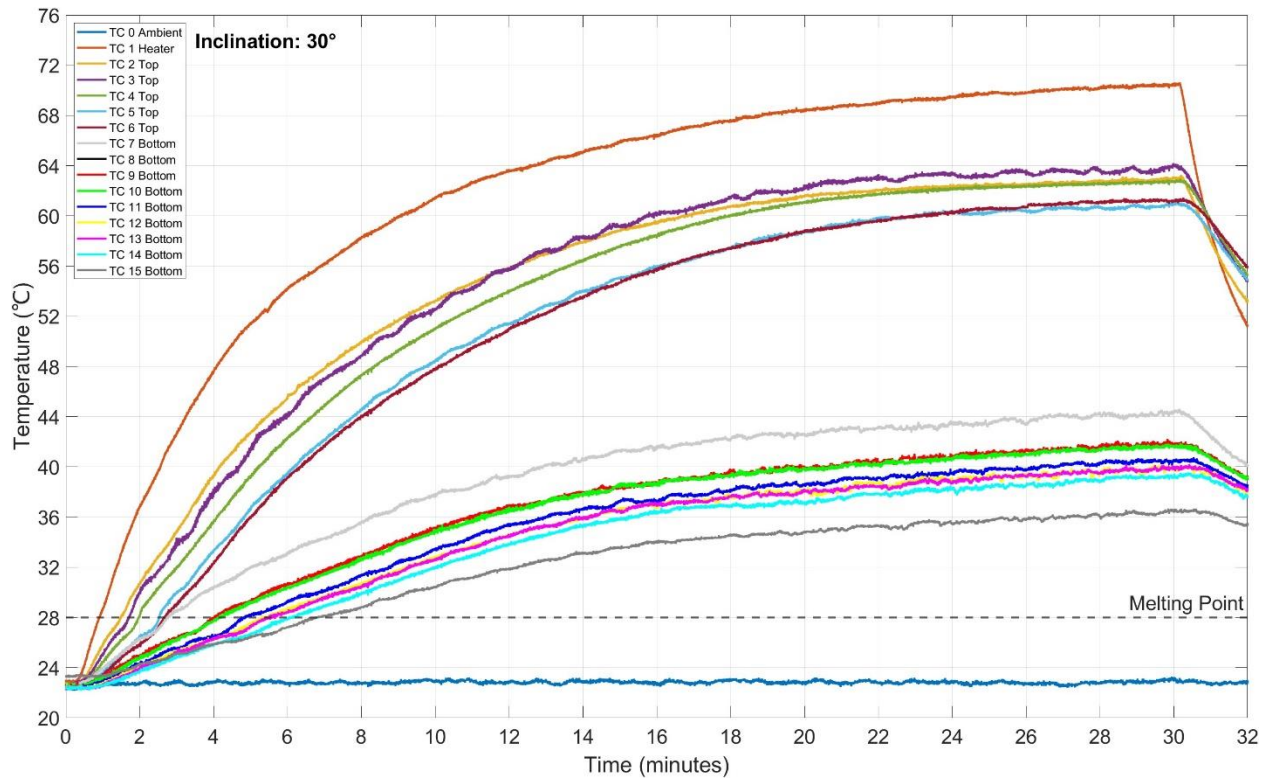


Figure 4.9: Temperature variations with time during Melting Without Vibration for the inclination angle of 30 degrees

4.1.5 Results for the Orientation Angle of 0°

In Figures 4.10 and 4.11, instantaneous photographs of the front observation window of the experimental set-up obtained at various time instants 0, 2.5, 5, 7.5, 10, 12.5, 15, 17.5, 20, 22.5, 25, 27.5 and 30 minutes are shown. The temporal variations of temperatures corresponding to case of Figure 4.10 are presented in Figure 4.12. The lowest and highest registered temperatures correspond to the lab environment and thermocouple embedded in the heated aluminum plate on the far-left hand side, respectively. The laboratory environment temperature remained fairly constant, whereas the temperature of the heated plate rose continuously during the heating period. The melting temperature of the PCM is also drawn as a dashed line. In between these two extreme temperatures, banding of measured temperatures on the top (5

curves) and the bottom (8 curves) aluminum plates are clearly noted. Inspecting photographs taken at time instance of 5 and 10 minutes, domination of heat conduction and heat transfer during the early period of heating is clearly evident due to progression of the liquid-solid interface as a straight vertical line. At the top of the LSI at 10 minutes, deviation from the vertical orientation suggests the slow dominance of natural convection. In fact, heated liquid PCM with the lower density would rise next to the heated plate and within sink along the LSI. During this time period of 10 minutes, melting of PCM next to the highly conductive top and bottom aluminum plates are also clearly observed in Figure 4.10.

Presence of a smooth surface at top of the LSI and a wavy bottom surface during late instants of melting are clearly observed. This difference between the melting patterns at the top and bottom of the receding solid PCM is related to dominance of two regimes in those zones. The convection field above the PCM in this configuration is related to a thermally stable layer, i.e. the hot lighter fluid is sitting at the top of the colder solid PCM. In contrast, with the enlarging liquid layer being formed above the bottom aluminum plate, a thermally unstable stable layer is being developed, i.e. the hot lighter fluid from the bottom aluminum plate rises toward the colder solid PCM. Thus, multicellular natural convection currents are active in melting and sculpting the observed wavy patterns.

0
min



2.5
min



5
min



7.5
min



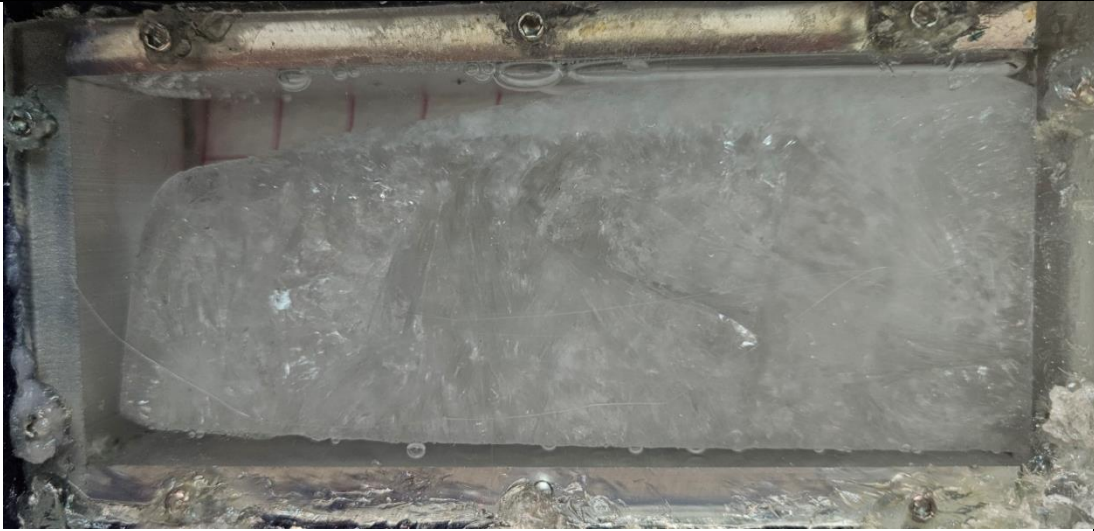
10
min



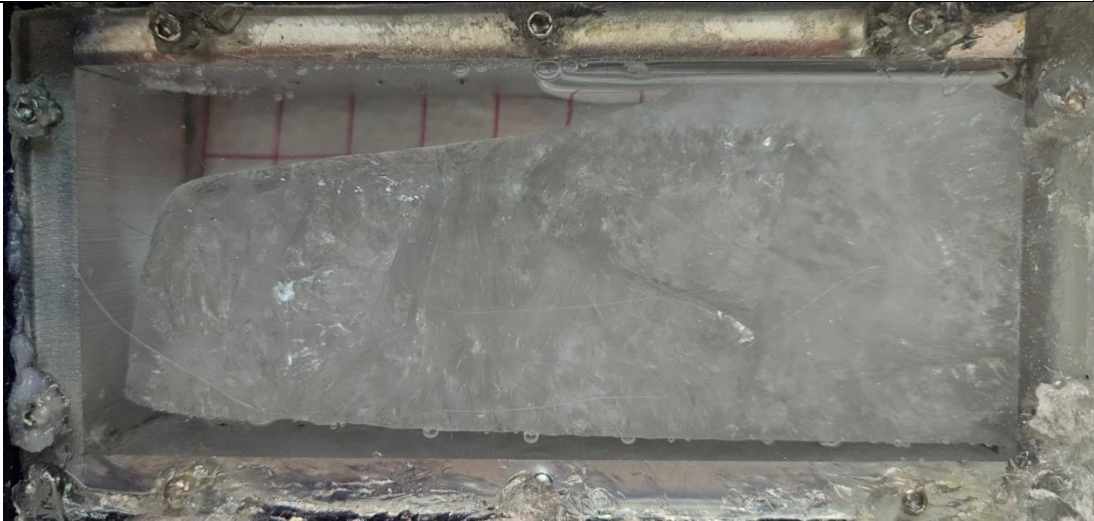
12.5
min



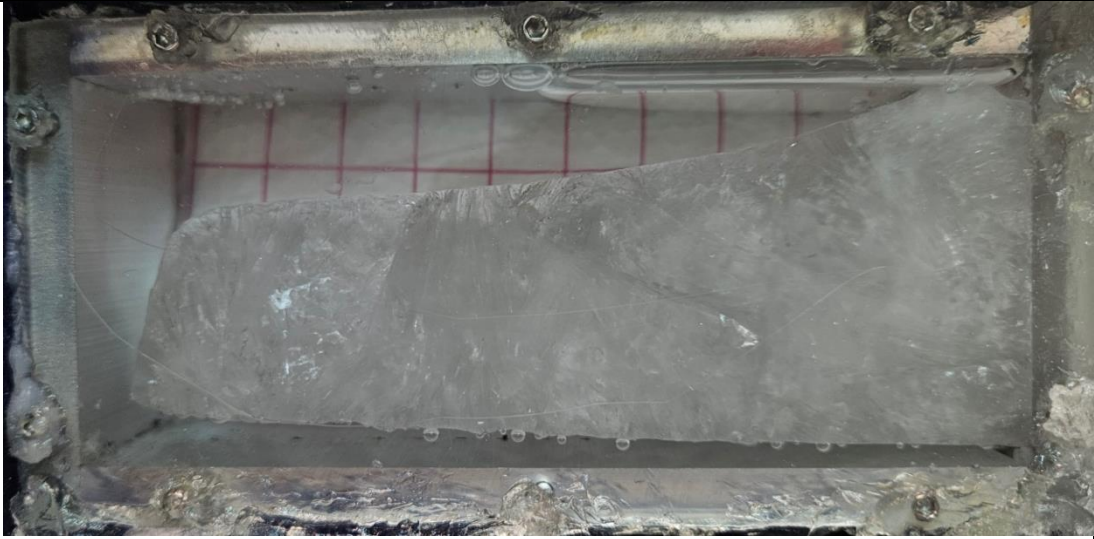
15
min



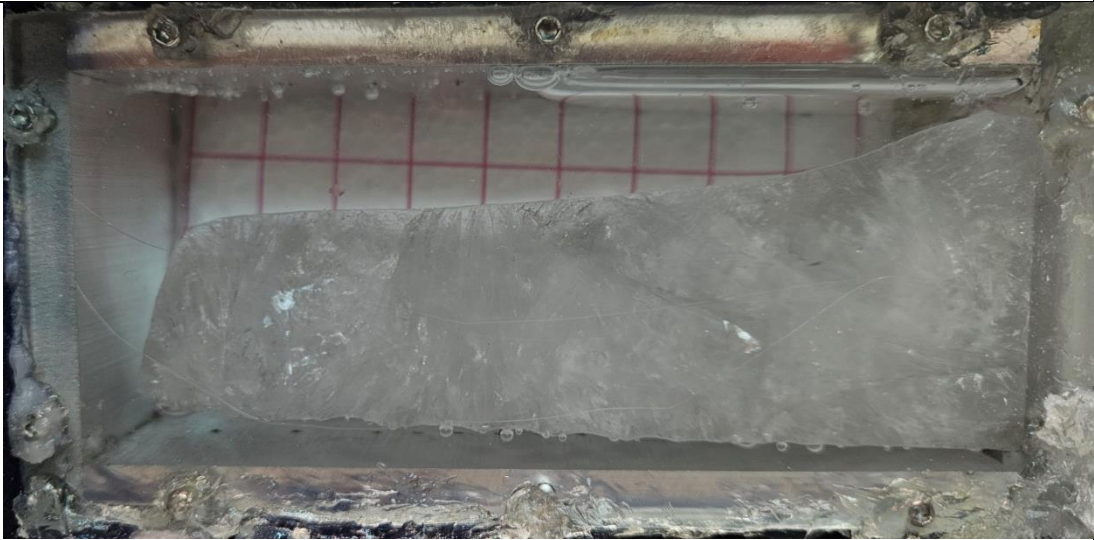
17.5
min



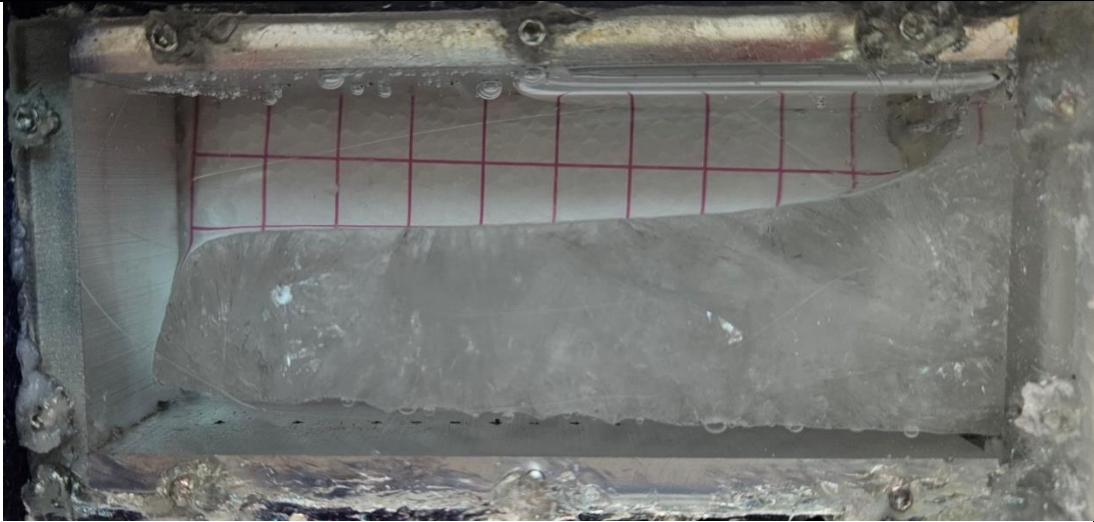
20
min



22.5
min



25
min



27.5
min

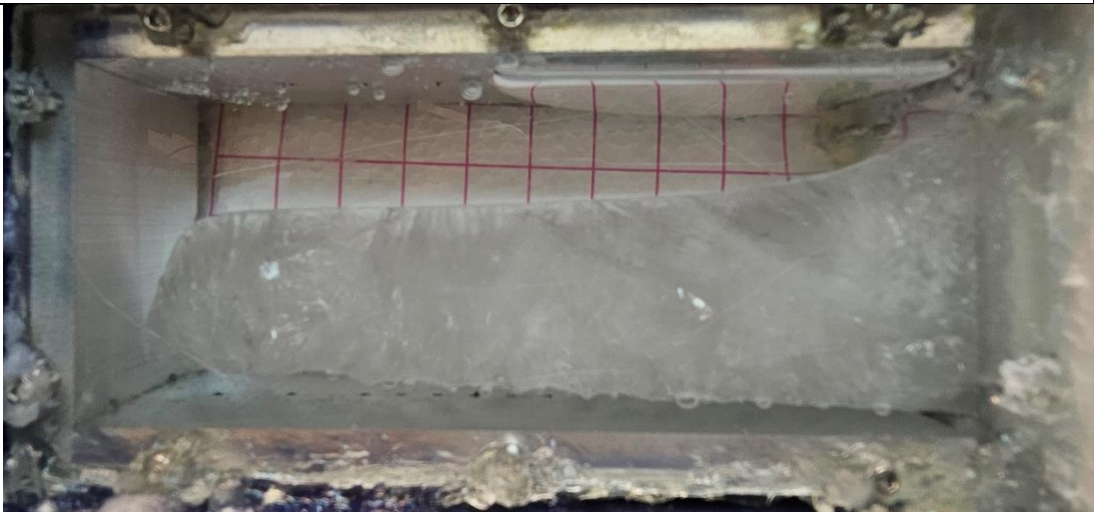




Figure 4.10: Instantaneous progression of the liquid-solid interface on the front observation window of the set-up during Melting Without Vibration for the inclination angle of 0 degrees (vertically-oriented heated plate on the far left)

Similar to the inclination angle of 90 degrees, a slanted view of the experimental set-up for the inclination angle of 90 degrees during heating is shown in Figure 4.11. This image exhibits that contrary to the assumed two-dimensional melting in such a system, there is marked 3-dimensional thawing inside the test cell.

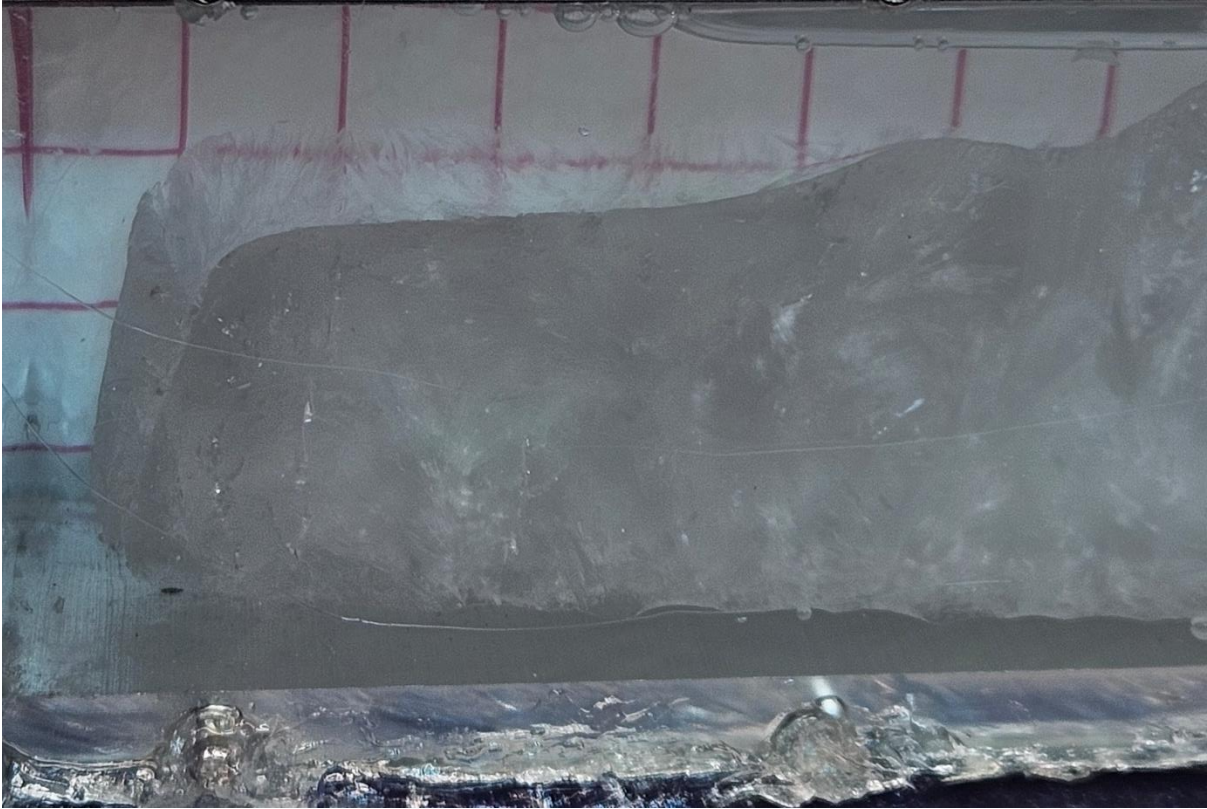


Figure 4.11: Slanted View for the Evidence of 3-Dimensional Melting ($t > 20$ minutes)

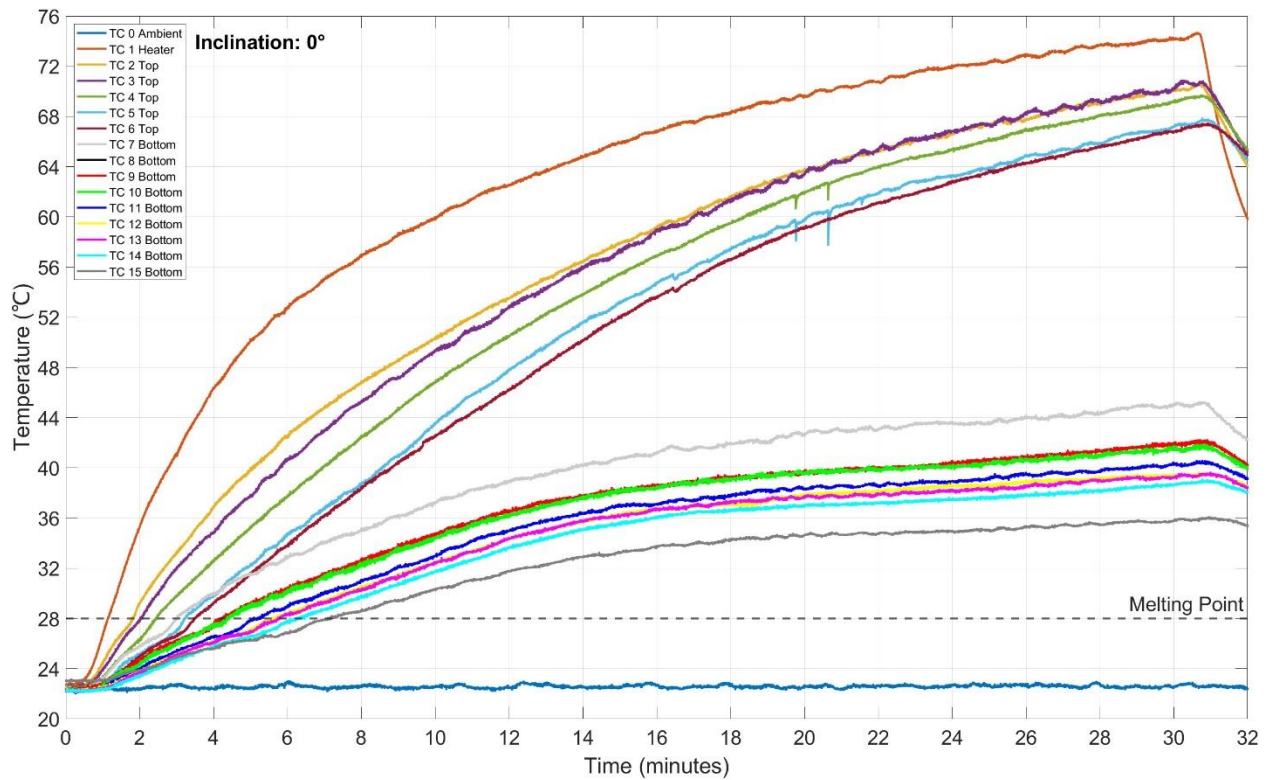


Figure 4.12: Temperature variations with time during Melting Without Vibration for the inclination angle of 0 degrees (vertically-oriented heated plate on the far left)

4.1.6 Estimation of the Melted Fraction (No Vibration)

Given the 3-dimensional uneven melting in the unit that was observed in Figures 4.2 and 4.12 corresponding to the inclination angles of 90 and 0 degrees, respectively, evaluation of the precise melting fraction in the unit complicated. The best way to do so is to take apart the container and measure the volume of liquid at various time instants, but the container being tested in this experiment was permanently sealed. Given this limitation, estimating the melting percentage was achieved by creating a grid pattern at the front observation window to calculate the volume or 'blocks' of material that have melted. This data are shown in Figure 4.13 suggesting that the 45 degree inclination angle exhibited the highest percentage of melting at the end of heating.

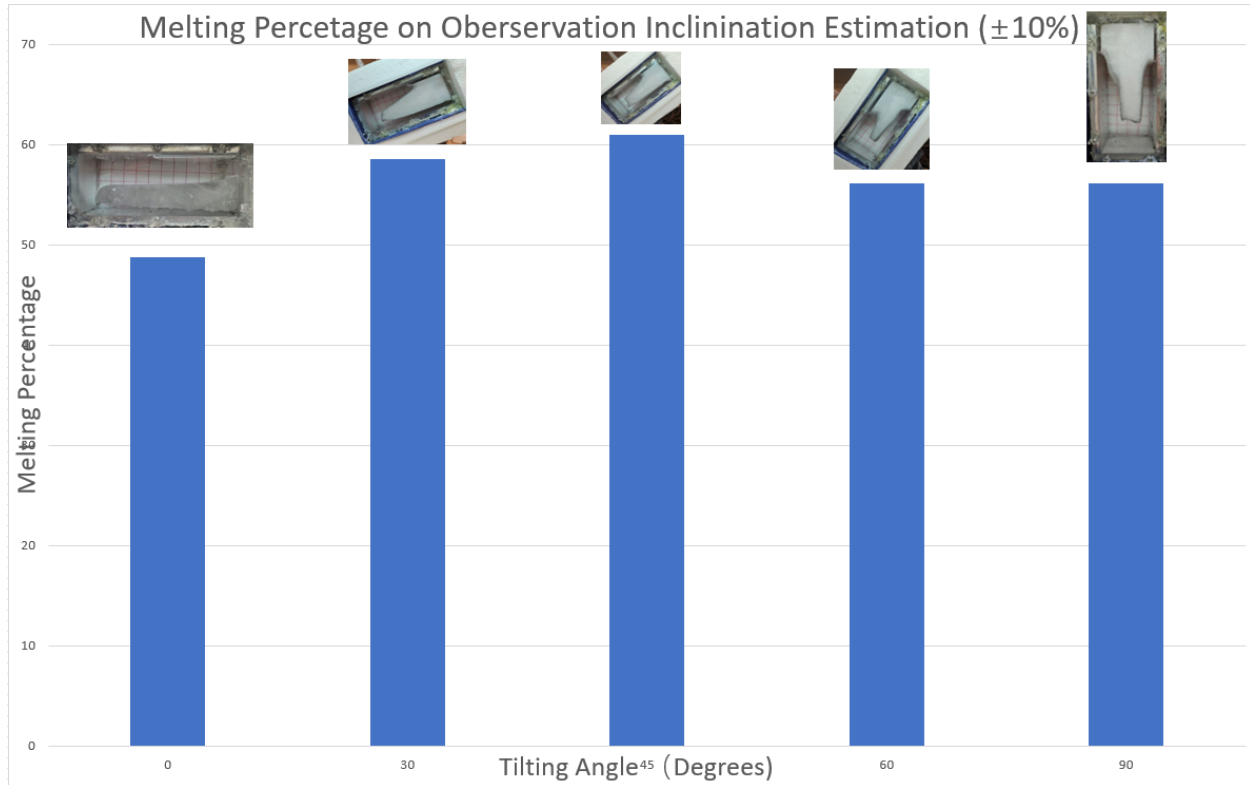


Figure 4.13 Estimated Melting Fraction Values without Vibration estimated from observation window images at the 30 minutes time instant

4.2 Estimation of the Rayleigh numbers

The presence and extent of the thermally unstable liquid layer formed between the bottom aluminum plate and the solid PCM for the case of inclination angle of zero (section 4.1.5) can be characterized via the non-dimensional Rayleigh number, i.e.:

$$Ra = \frac{g\beta(T_w - T_m)}{\nu\alpha} \quad (4.1)$$

where g is the gravitational acceleration (9.8 m/s^2), β is the thermal expansion coefficient (K^{-1}), T_w is the hot plate temperature (K) and colder melting temperature, T_m (K). The length L_c is the changing vertical distance (m) between the hot surface and the cold PCM material.

Furthermore, fluid kinematic viscosity, i.e. ν ($\text{m}^2 \text{ s}^{-1}$) is:

$$v = \frac{\mu}{\rho}, \quad (4.2)$$

where μ is the dynamic viscosity ($\text{kg m}^{-1} \text{s}^{-1}$) and ρ is the density (kg m^{-3}).

Thermal diffusivity, i.e. α ($\text{m}^2 \text{s}^{-1}$) of the PCM is:

$$\alpha = \frac{k}{\rho * C_p}, \quad (4.3)$$

where k is the thermal conductivity ($\text{W m}^{-1} \text{K}^{-1}$) and C_p is the specific heat (kJ/ kg K^{-1}). The Rayleigh number, being a non-dimensional parameter, is a measure of the interplay between buoyancy driven and viscous forces.

In our estimation, T_m is the melting temperature of the PCM, i.e. 28°C (301.15K), whereas the hot plate temperatures can be determined by the instantaneous reading from thermocouples (TC 7-15) in Figure 4.12. The vertical liquid distance between the bottom aluminum fin and the unmolten PCM above the functioning thermocouples at various time points were estimated from the experimental recordings of Figure 4.10. The time variations of the Rayleigh numbers evaluated above each of the thermocouples 7-15 (excluding thermocouple 8 that failed before tests) are shown in Figure 4.14. All values of the Ra rise from initial values of zero toward higher values as the temperature difference is increased and the vertical liquid spacing widens. At any given time instant, the Ra number is highest for the liquid above the thermocouple that is nearest to the heated plate. The maximum Ra values are of the order of 2500 that is in the laminar regime.

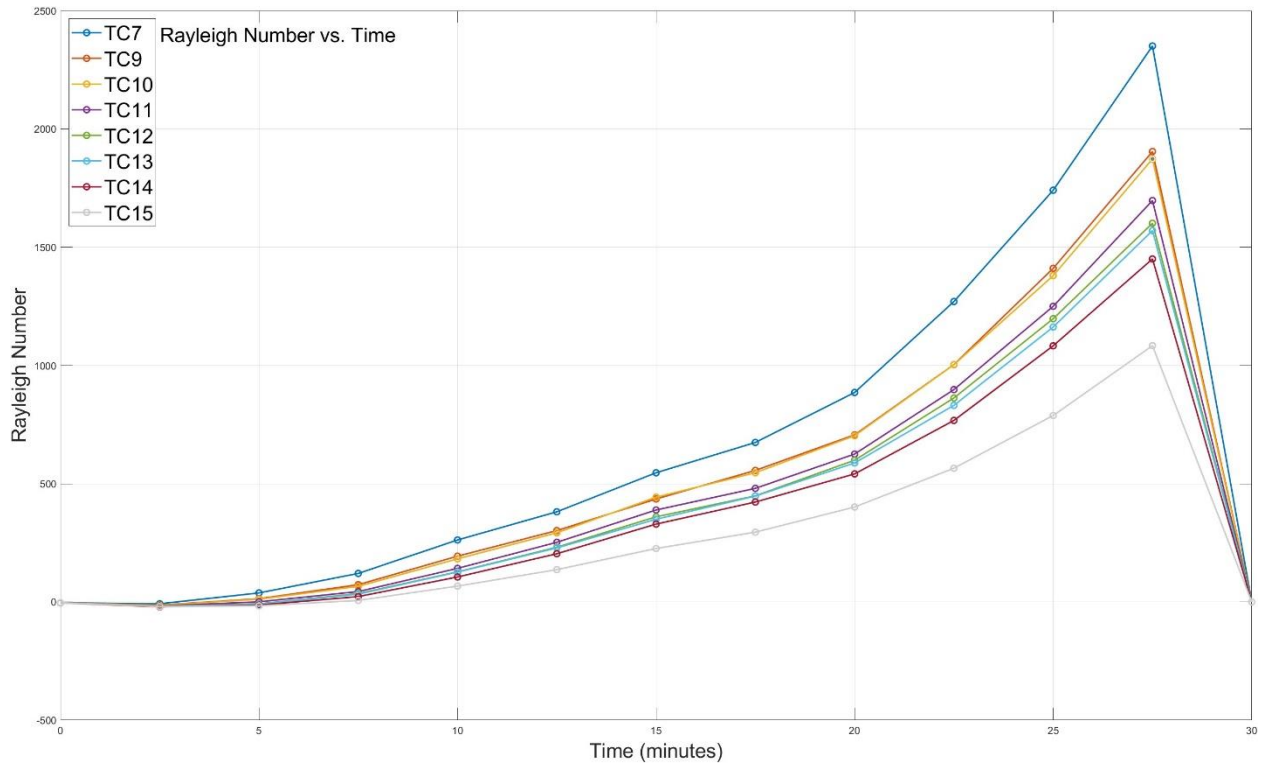


Figure 4.14 Estimated values of the Rayleigh numbers above thermocouples 7-15 for the inclination angle of 0 degrees

4.3 Power Delivered to the System

The power that can be delivered from the AC variac is of the order of 40 W, but in reality, due to the instrument ability, we are turning it to around 110V ac, current are measured to be 0.31 amp for every run. Figure 4.15 shows the reading from the instrument. The equation for calculating the AC power is:

$$AC\ Power\ (W) = Voltage\ (V) * Current\ (A) * PowerFactor(PF) \quad (4.4)$$

However, since the measuring device was picking up the number directly from the heater instead of the power supply, so the power factor can be ignored in this case, and equation 4.4 can be simplified to equation 4.5 as shown below:

$$AC \text{ Power (W)} = \text{Voltage (V)} * \text{Current (A)} \quad (4.5)$$

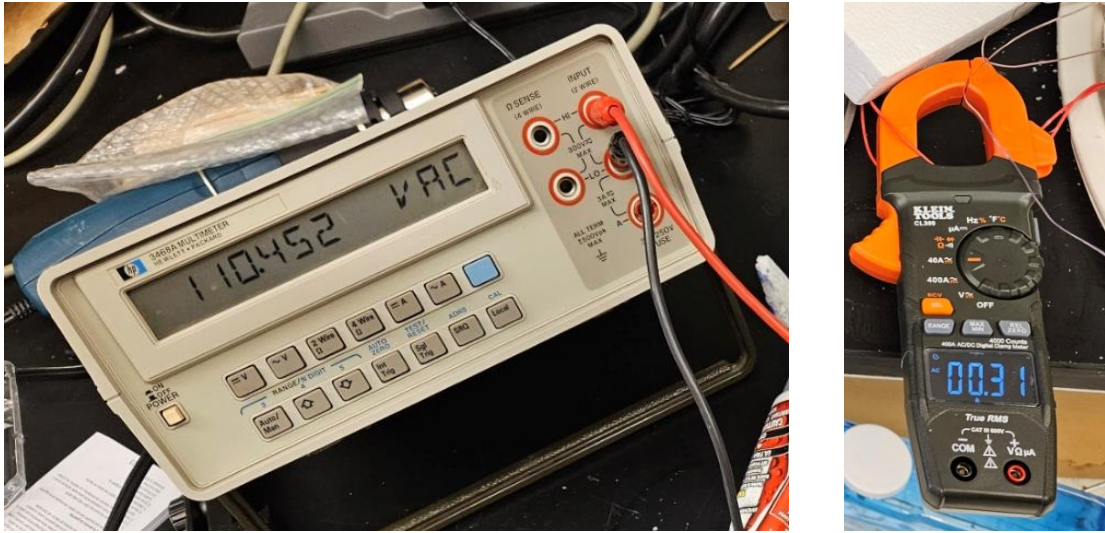


Figure 4.15: Multimeter Read out for voltage and current

4.4 Experimental Data for Cases with Vibration

For cases involving mechanical vibrations, the test cell under two extreme configurations, i.e. (a) 0-degrees and (b) 90-degrees were tested.

In this section, melting of the PCM within the test cell for inclinations angles of 0 degrees , with vibration frequency 50 Hz and 100 Hz at 1G acceleration will be discussed. The frequency was chosen due to the report of USABC report on their testing for the car battery and 1G acceleration was chosen due to the limitations of instrument and equipment.

4.4.1 Results for the Orientation Angle of 0° with Vibration at 50 Hz (1G)

Instantaneous photographs of the front observation window of the experimental set-up obtained at 2.5 minutes intervals from start of heating and ending at the 30 minutes time instant for the vibration at 50 Hz (1G) case with inclination angle of 0 degrees are shown in Figure 4.16.

The corresponding temporal variations of temperatures to case of Figure 4.16 are presented in Figure 4.17.

A large quantity of fluid was lost due to the container leakage so the top plates' thermocouples are not measuring the PCM but rather hot air or the aluminum plate. At same time, the lesser amount of fluid caused the overhang as shown in figure 4.16 around 22 minutes. The overhang broke off around 22.5 minutes right after the photo was taken. It is evident from the thermocouple reading around that time where the temperature drop happens. The best explanation of which is that cold PCM solid drop into the hot PCM fluid has cool down the fluid by the melting event.

Meanwhile, the bottom of the PCM was exhibiting the greatest waviness so far among all of the experiments which have been performed so far.



2.5
min



5
min



7.5
min



10
min



12.5
min



15
min



17.5
min



20
min



22.5
min



25
min



27.5
min



30
min



Figure 4.16: Instantaneous progression of the liquid-solid interface on the front observation window of the set-up during Melting Without Vibration for the inclination angle of 0 degrees with Mechanical Vibration at 50 Hz (1G) (vertically-oriented heated plate on the far left)

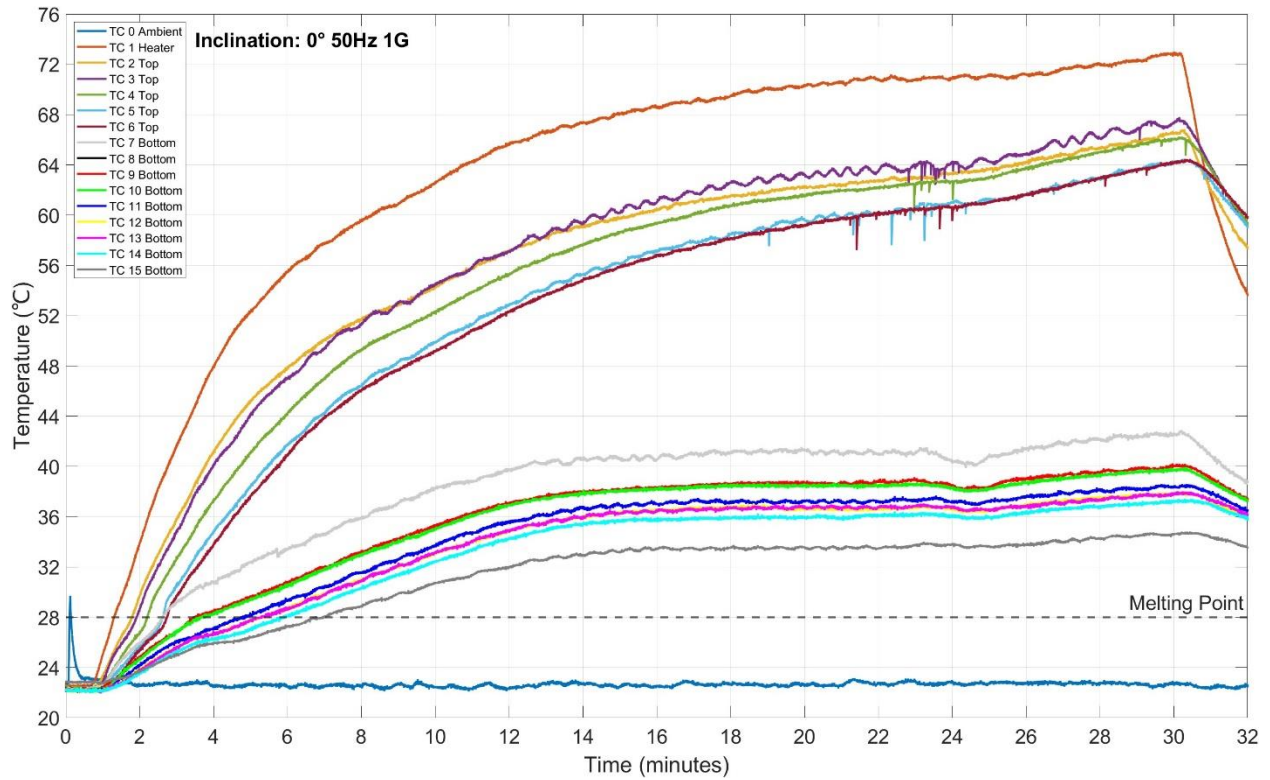


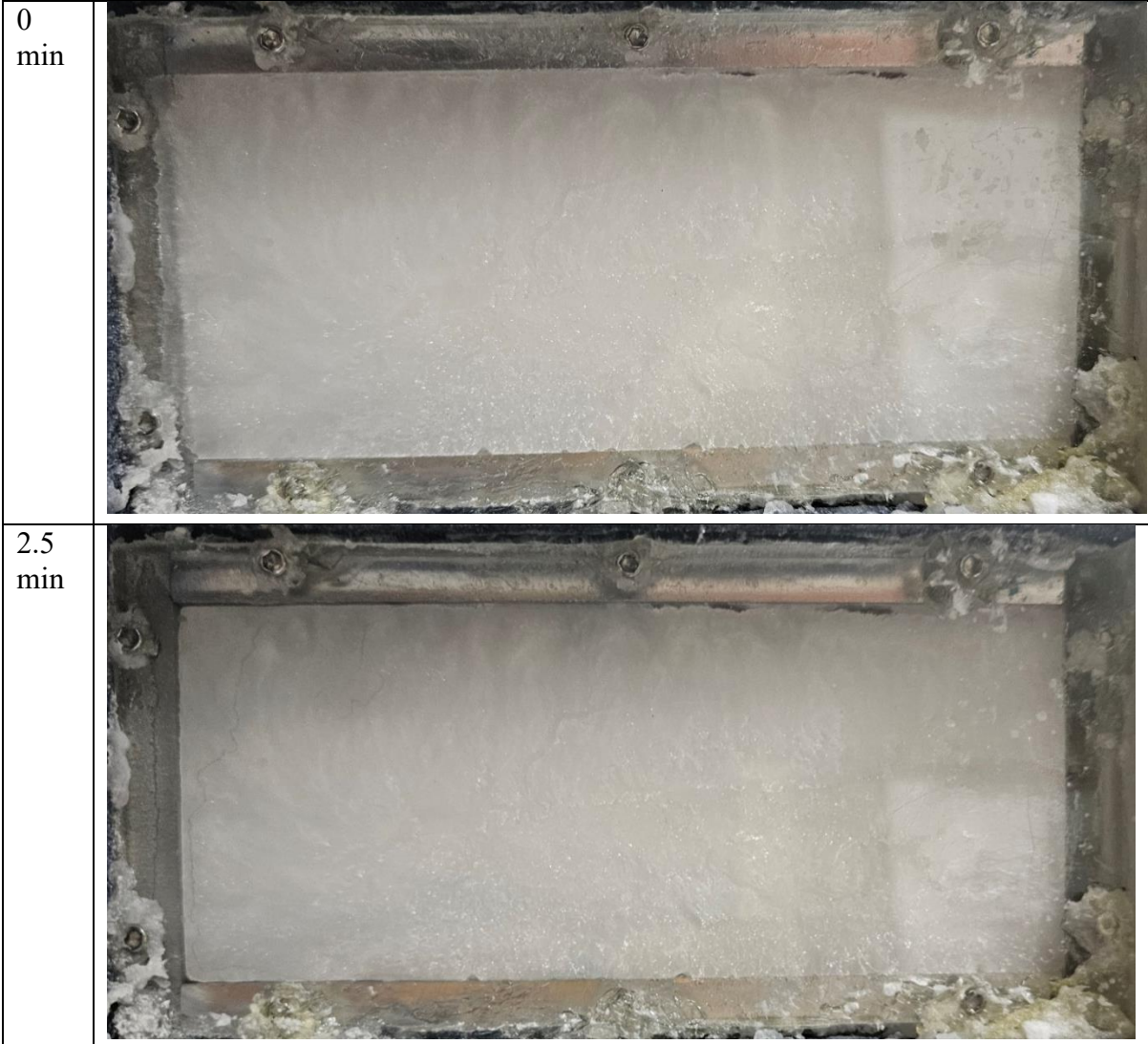
Figure 4.17: Temperature variations with time during Melting With 50 Hz (1G) Mechanical Vibration for the inclination angle of 0 degrees (vertically-oriented heated plate on the far left)

4.4.2 Results for the Orientation Angle of 0° with Vibration at 100 Hz (1G)

Instantaneous photographs of the front observation window of the experimental set-up obtained at various time instants of 0, 5, 10, 15, 20, 25 and 30 minutes for the vibration at 50Hz 1G case with inclination angle of 0 degrees are shown in Figure 4.18. The corresponding temporal variations of temperatures to case of Figure 4.18 are presented in Figure 4.19.

A similar overhang was also observed in this experiment case, causing the top plate measurements to be meaningless. Using the relation for acceleration, at the same acceleration level, higher the frequency lower the amplitude, from the liquid surface, clearly at 100Hz 1G, the

wave was lower than the one in 50Hz 1G test, the bottom of the material also gets less waviness in this case.



5
min





7.5
min



10
min



| | |
|-------------|--|
| 12.5 min |  |
| 15 min |  |
| 17.5 min |  |

20
min



22.5
min



25
min



27.5
min





Figure 4.18: Instantaneous progression of the liquid-solid interface on the front observation window of the set-up during Melting Without Vibration for the inclination angle of 0 degrees with Mechanical Vibration at 100 Hz (1G) (vertically-oriented heated plate on the far left)

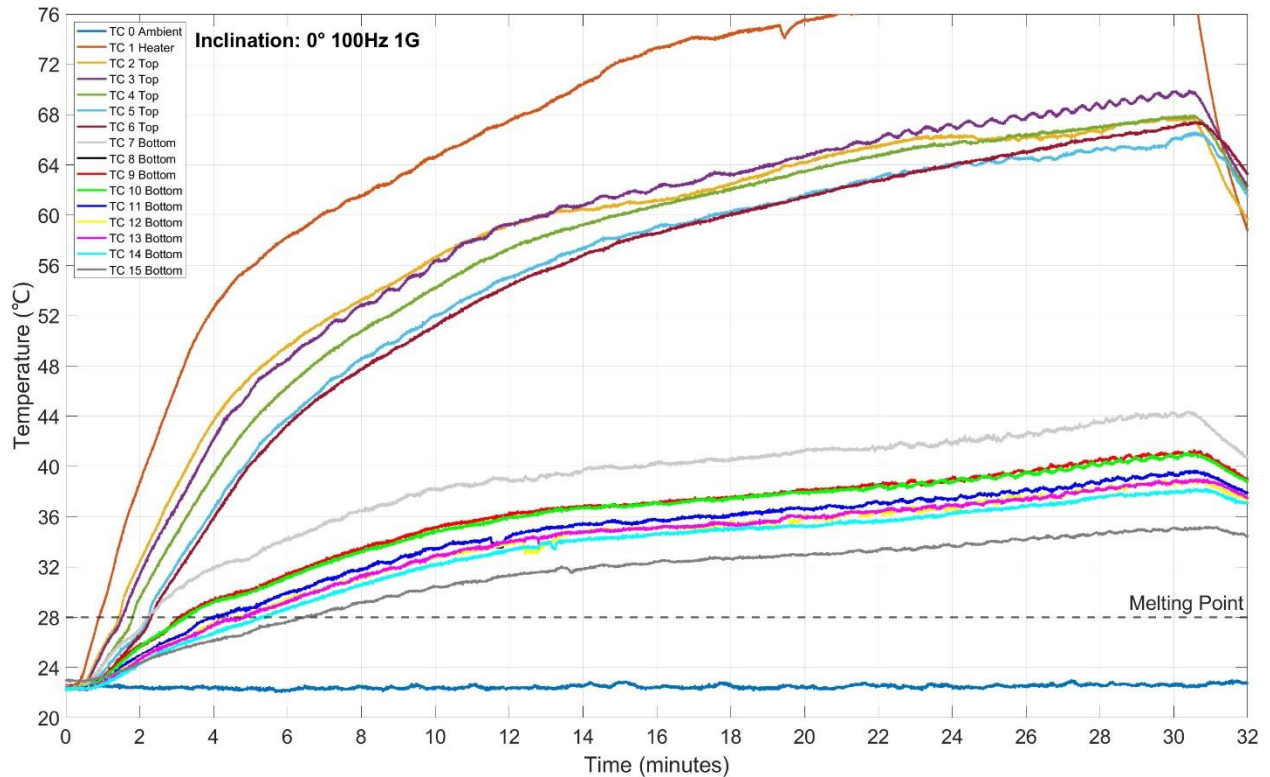


Figure 4.19: Temperature variations with time during Melting With 100 Hz (1G) Mechanical Vibration for the inclination angle of 0 degrees (vertically-oriented heated plate on the far left)

4.5 Variations of the Heater Plate Temperatures

The test cell is operated by a constant heat input on the heated plate, differentiating it from a constant-temperature operation. Variations of the temperature of the thermocouple embedded into the heated plate for different orientation angles of 0, 30, 45, 60 and 90 are plotted next to each other in Figure 4.20. With the PCM initially at its solid state and conduction the dominant mechanism upon melting, the variations of temperatures corresponding to different inclination angles are nearly identical during the early duration of heating ($t < 2$ min). Thereafter, the registered temperatures exhibit dependence of orientation angle signifying influence of the emerging convection fields on the system.

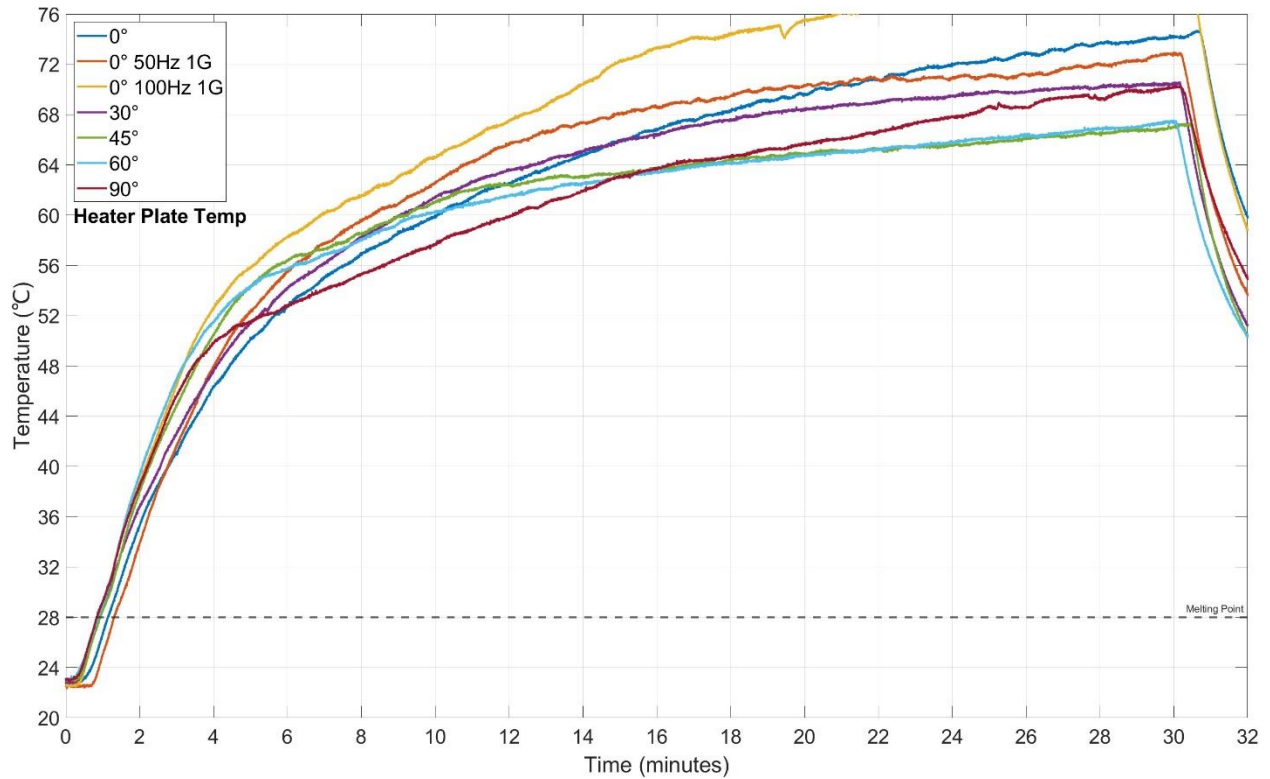


Figure 4.20: Variations of the Heated Plate Temperatures for various inclination angles

4.6 Estimated Melting Fraction

The 3-dimensional uneven melting makes it hard to calculate the precise melting fraction. Best way to do so is to take apart the container and measure the volume of liquid, but the container being tested in this experiment was permanently sealed. Melting percentage was estimated using the grid at back and another grid was created at the front observation window to calculate the volume or ‘blocks’ of material that has melted (Figure 4.21).

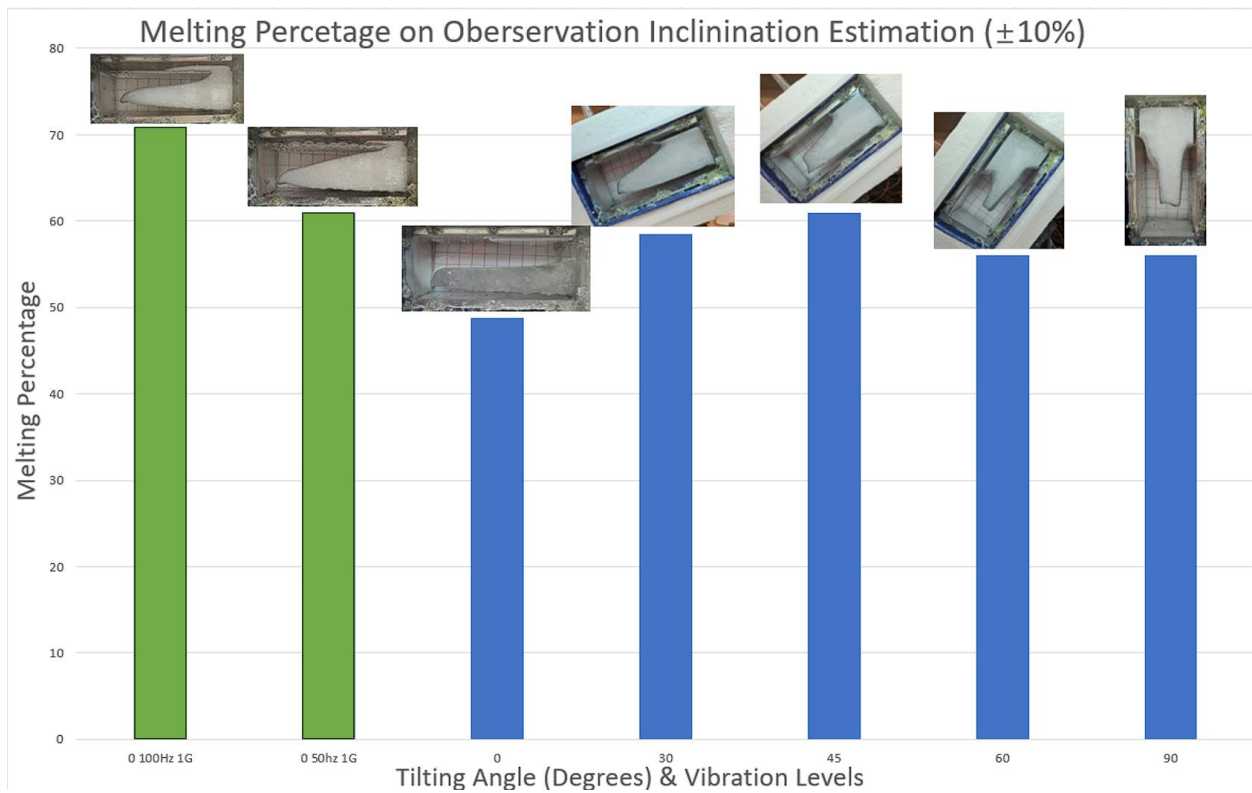


Figure 4.21: Estimated Melting Fraction Chart with Vibration Cases

Chapter 5 Conclusions and Recommendations

Conclusions arrived at in the course of this experimental investigation are outlined and a few recommendations for future researchers who might have interest on repeating this experiment are provided below.

5.1 Conclusions

With the system subject to no mechanical vibrations, the major findings are:

1. From the experimental data and visual observations of the transparent access window, we can conclude that for the exact same rectangular container and for the same amount of heat flux input, a container will melt most by setting it at an inclination of 45 degrees.
2. Simultaneously, strong three-dimensionality on other planes normal to the observation window were noticed that could only be accessed qualitatively.
3. Despite liquid leakage from the cell and persistence of bubbles above molten liquid, thermocouples responded very well.

Upon subjecting the unit to mechanical vibrations:

4. The melting process was further enhanced. At the same acceleration level, the higher the frequency, the lesser amplitude and lesser distraction will apply to the material but will generate a faster melting curve.

5.2 Recommendations

- 1) Cut-out grooves on the side of plate can be machined so that rubber O-rings can be placed between container pieces for better sealing.
- 2) Using the flex seal with even higher rating and flexibility of which is also important due to the thermal expansion during the experiment.
- 3) Building a smaller container allows faster melting and cooling phase, so a single container will be enough for rapid testing.
- 4) When applying in the seal glue, try use thermal paste to minimize the possible cause of change the thermal conductivity between two metal fins, while applying the sealant on the outside of the container rather in the gap between the plates.

References

Bošnjaković, M. and Tadijanović, V., 2019. Environment impact of a concentrated solar power plant. *Tehnički glasnik*, 13(1), pp.68-74.

Eftekhar J, Haji-Sheikh A, Lou DYS. Heat transfer enhancement in a paraffin wax thermal storage system. *Journal of Solar Energy Engineering* 1984;106:299–306.

Haji-Sheikh, A., Eftekhar, J. and Lou, D. Y. S.. Some Thermophysical Properties of Paraffin Wax as a Thermal Storage Medium, in *Spacecraft Thermal Control, Design, and Operation*, Vol. 86 of *Progress in Astronautics and Aeronautics*, AIAA, New York, New York, 1983, pp. 241-253.

Henze, R.H. and Humphrey, J.A., 1981. Enhanced heat conduction in phase-change thermal energy storage devices. *International Journal of Heat and Mass Transfer*, 24(3), pp.459-474.

Joshy, N., Hajiyan, M., Siddique, A.R.M., Tasnim, S., Simha, H. and Mahmud, S., 2020. Experimental investigation of the effect of vibration on phase change material (PCM) based battery thermal management system. *Journal of Power Sources*, 450, p.227717.

Lee, H. and Han, J.H., 2022. Experimental Study on the Melting Behavior of a Phase Change Material under Random Vibration. *Experimental Heat Transfer*, pp.1-21.

Scammel, A. Development and Testing of a Foam Matrix and Phase Change Material Composite, Internal Report, Auburn University, 2011.

Vadasz, J.J., Meyer, J.P., Govender, S. and Ziskind, G., 2016. Experimental study of vibration effects on heat transfer during solidification of paraffin in a spherical shell. *Experimental Heat Transfer*, 29(3), pp.285-298.

Appendices

Appendix A: Thermocouple Preparation and Calibration

The processes for making T-type thermocouples begin with getting the proper wire (Figure A.1).



Figure A.1: T-type Thermocouple Wire

Once we have the proper wire, we striped away the insulation with a wire stripper (figure A.2).



Figure A.2: Stripping the Insulation with the Wire Stripper

Then, we put a small hex key between two wires in order to form a loop. Once that is done, a piler tool is used to tie the two wire together on one end of a wire. Cut away any excessive wire after where the tie was formed, the result of this looks like figure A.3 shown below:

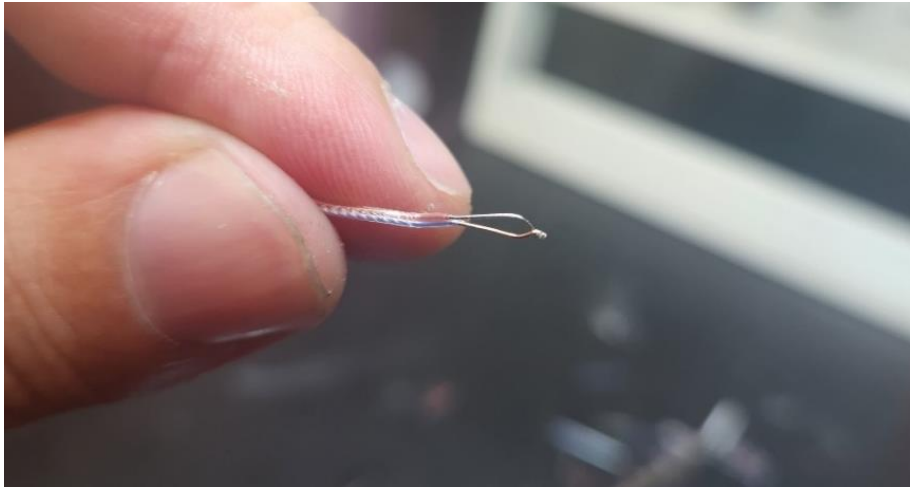


Figure A.3: Tie Thermocouple Wire

With everything above done, we use a thermocouple welder (figure A.4), to form the testing beads of the thermocouple (figure A.5).

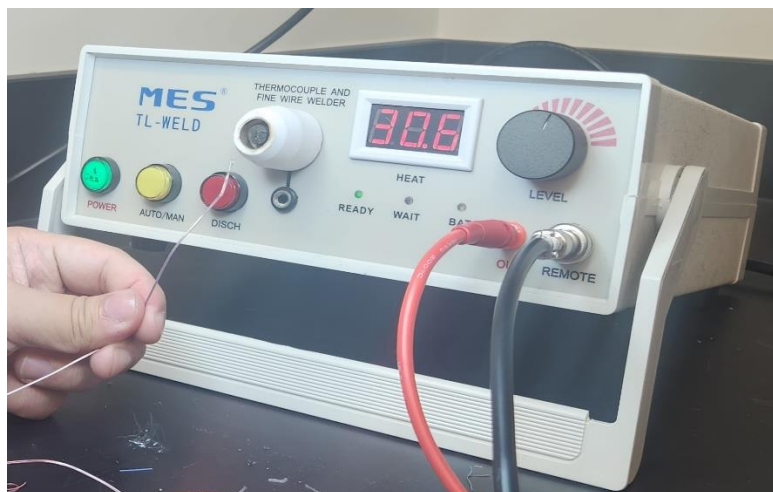


Figure A.4: Welding the Thermocouple Wire

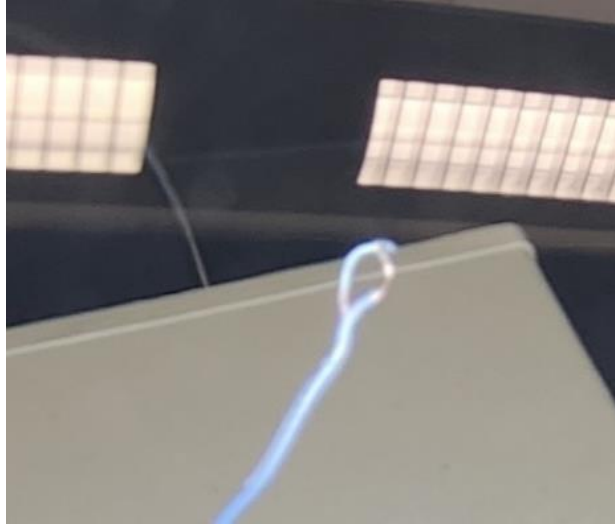


Figure A.5: Thermocouple's Beads

Once the wires were made, a quick test was conducted with a special plug (figure A.6),

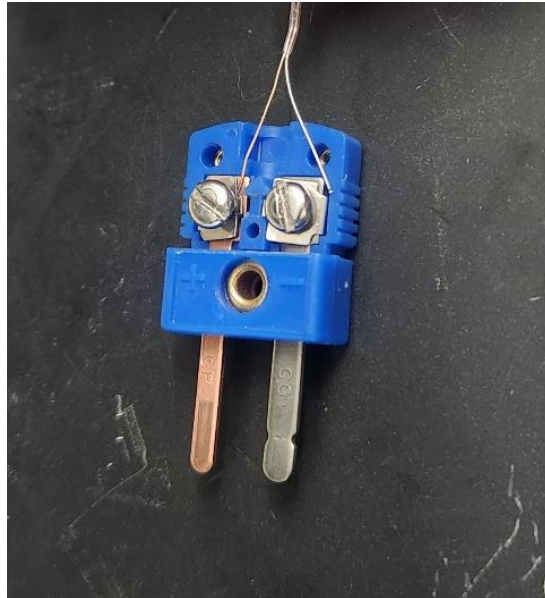


Figure A.6: Testing Plug

Insert two wires of thermocouple into this plug and place it into the multimeter. Put the thermocouple beads into both ice point machine and heat point machine (figure A.7), which provide a constant around 0- and 100-degree Celsius temperature for testing.



Figure A.7: Testing with Ice point and Hot point Cell

Finally, the exposed wires will be wrapped by epoxy (figure A.8) to ensure they will be sealed and insulated nicely and they will be ready for the next step



Figure A.8: Thermocouple Head Sealed with Epoxy

Once the thermocouple was made, it need to be calibrated so they can report the temperature properly.

The process of calibration is critical for any measuring equipment.

The calibration was done with a water bath and a calibrated GE thermistor (figure A.9). The GE thermistor could not connect to a data acquisition system to PC for recording, so we used a multimeter to record the resistance report by the thermistor (figure A.10).

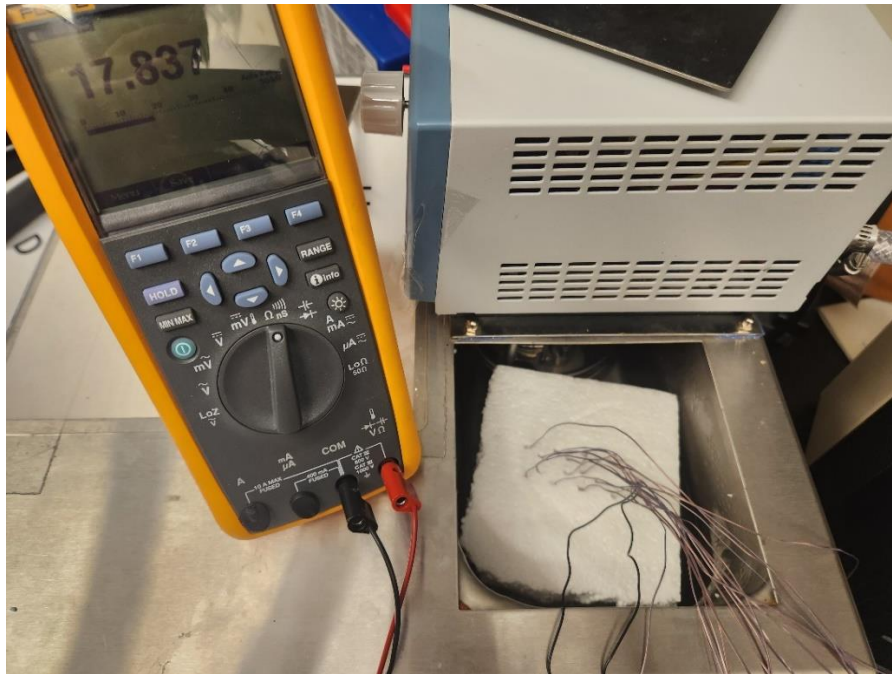


Figure A.9: Thermocouple Calibration

The process is to set the water bath temperature at every 10 degree from 10 to 80 Celsius. Once the water bath reaches our goal temperature and the reading on its panel become constant, we start our recording for both the multimeter and data acquisition system. We will ran it for 5 minutes minimum and take the last 3 minutes average as our result. The sampling rate for multimeter was set to be every 0.1 s and thermocouple was also set to be 0.1 s.

Once we have all the data collected, we compute the actual temperature from the thermistor since the read out is still in voltage rather than temperature. Then we compare each thermistor temperature with thermocouple temperature read out and form a graph similar to figure A.11.

As soon as we have the chart, this means our calibration is complete. For any temperature reading we get from the thermocouple, we just need bring it to this chart and we will be able to find the correct temperature easily.



Figure A.10: Read out from the thermistor

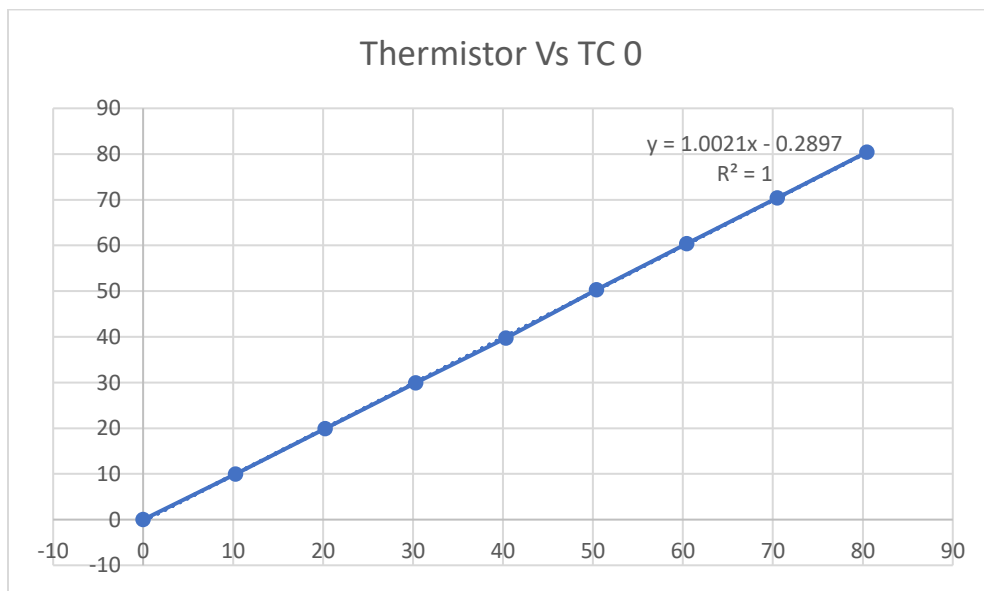


Figure A.11: Example of Temperature Calibration Chart

Appendix B: Preparation of the PCM Container

The material chosen was a 0.25 inch 6061 aluminum plate and 0.25 inch Plexiglas.

A Maxiém 1515 Water jet was utilized in this case for cutting the material (Figure B.1).

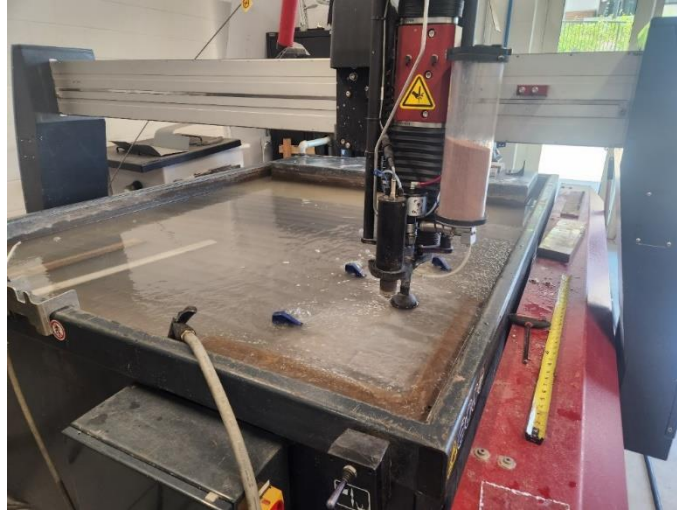


Figure B.1: Water Jet in Cutting Operation

The machine delivers an accurate cut to the level of ± 0.003 inch. Once the material gets cut, we used a Precision Matthews PM-950S knee mill, to find the precise location for all the holes on our plates where it needs to be drilled (figure B.2).



Figure B.2: Drilling and Fining Material with Manual Mill

This mill gives us a machining accuracy to ± 0.0001 inch (figure B.3).

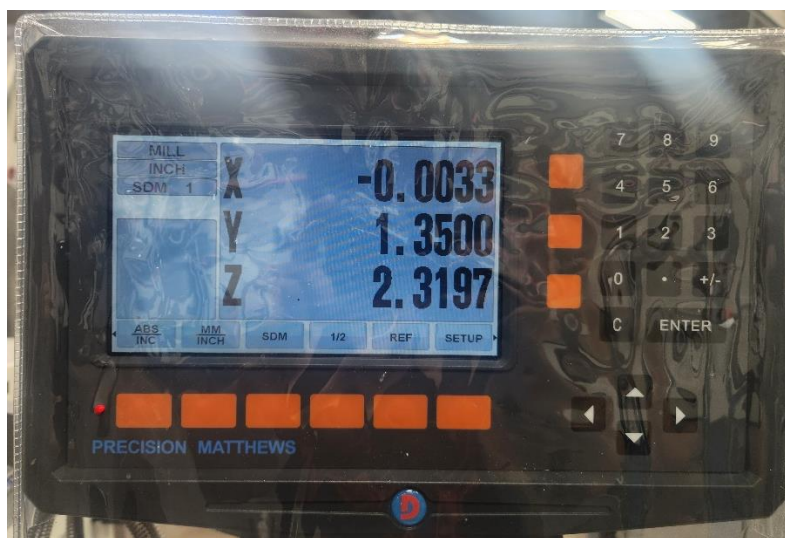


Figure B.3: Digital Read Out for the Manual Mill

Once all the pieces were made, we inserted the thermocouple wires into drilled holes on the metal plate and sealed them with silicone rubber and epoxy (figure B.4).

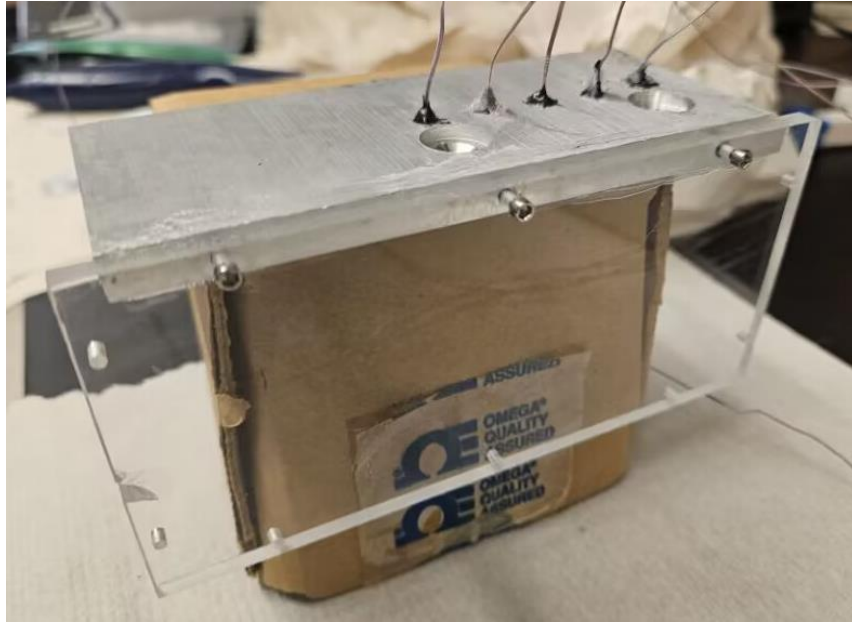


Figure B.4: Thermocouple Glued to the Plates

With all the thermocouples inserted and glued, we can now start gluing the container together with epoxy and other sealing materials. We glued five side together and leave one side open for PCM filament purposes (figure B.5).

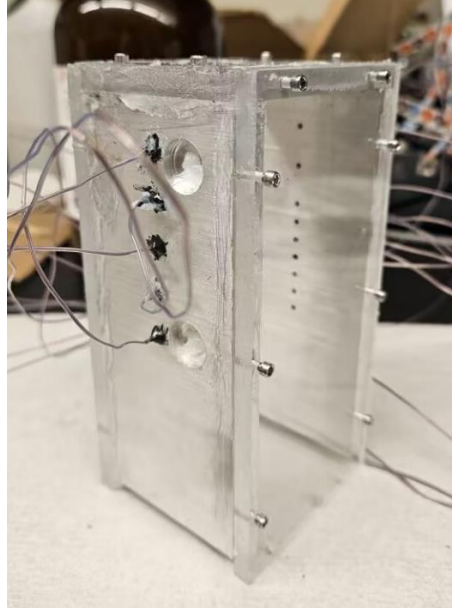


Figure B.5: Assembled Container

A water leakage test was conducted after the container was assembled to inspect the container if it has any leakage so we can prevent it happening before filling in PCM (Figure B.6).

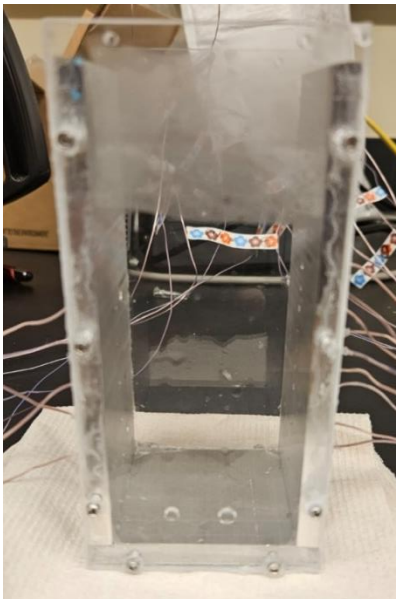


Figure B.6: Sealed Container Right After Leaking Test

Appendix C: PCM Filling Process

The filling process began with heating up all the materials and the container. We heat up all the container and equipment such as funnel and beaker to 45 °C and used a Binder ED23 oven to do so. All equipment will sit inside there for a day and we start the pouring process the next day. (figure C.1).

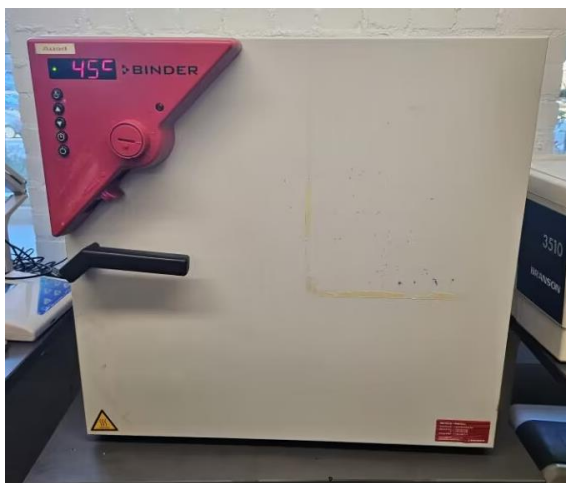


Figure C.1.1: Binder Oven



Figure C.1.2: All Equipment and PCM Sitting Inside the Oven

Once we have everything heated for a day, we turn a heat plate on to let the container be warm as possible while we are pouring. Then we first pour our material into a beaker for easier handling purpose. Then we use a funnel to guide the PCM liquid and pouring from the bottom of the container, which reduces the shock of PCM and trap as less as air possible even during the pouring process (figure C.2).



Figure C.2: Pouring the PCM

Once the pouring is done, PCM container will be sit inside a VWR 1430M vacuum oven for 24 hours of degassing process at 45°C (figure C.3). The pressure and temperature settings were at 25mm Hg, respectively.



Figure C.3: VWR 1430M vacuum oven

After 24 hours of vacuum process, we turned off the heat and let the container set inside the oven for another 24 hours to solidify. And the outcome is shown in figure C.4.



Figure C.4: PCM Solidify after 24 hours.

From the figure, it is not hard to tell, when a material solidifies, the size shrink as density goes up, so to full fill the container, a second pouring will be necessary (Figure C.5).



Figure C.5: Second Pouring Done

Once the second pouring is done, repeat the degassing process but turn the heat off so it will not melt and cause expansion of the previous poured material. Once this step was completed, the container with PCM will be ready (figure C.6).



Figure C.6: PCM Pouring Process Done

An interesting find during the cool-down process is that instead of turning off the oven, if we turn the temperature down to 35 °C for 24 hours, then we turn the heat completely off and let it cool down to room temperature for another 24 hours, we will have a different result on the PCM, it turns out to be almost clear instead of the hard see through status. But consider the fact that we have no control over the cooling temperature once the experiment starts and we are not certain if the different color of PCM will also have different physical properties. We heat the material up once again and cools it down right away.



Figure C.7: Solid PCM When Using Step Down Cooling

Appendix D. Building and Assembly of the Final Test Bench

Model was created in SolidWorks and used a 3D resin printer to print out pieces which make sure they will be able to sustain heat during our experimental process.

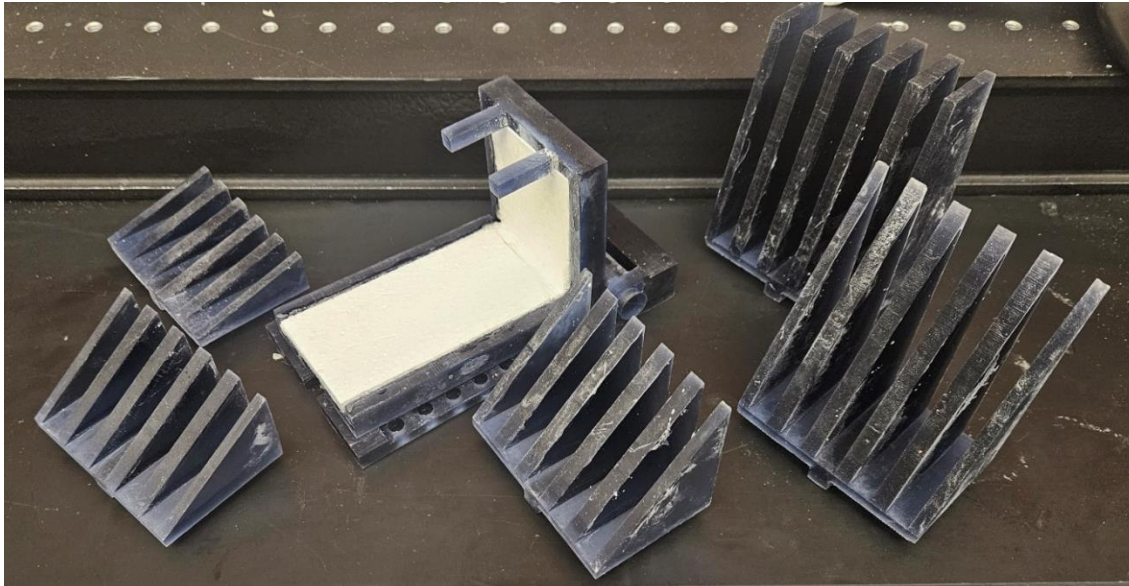


Figure D.1: Print Out Pieces

While the testing container is ready, although we are ignoring the effects of the environment, but heat loss via radiation and conduction are existed and will a great heat loss will cause error and other problems during our experiments. So a certain amount of insulations will be necessary for our container to isolated it as much as possible from the surrounding. So we cut some foam board pieces with the hot wire knife (Figure D.2).

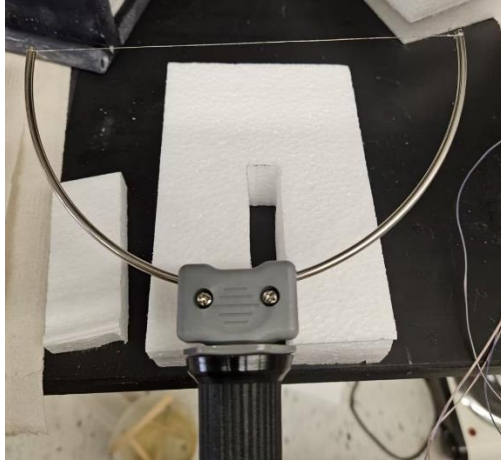


Figure D.2: Hot Wire Knife and Foam Piece

Then glued them to the container, with mat sheet in between, and use zip lock to tie everything down to the bottom, to make sure the container was secured even during our mechanical vibration test (Figure D.3).

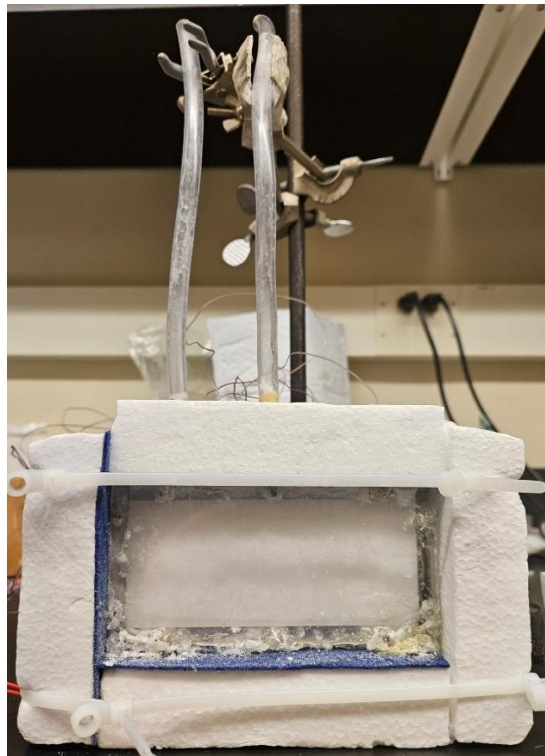


Figure D.3: Full Test set-up

Appendix E. Thermocouple Testing Bead Shape Effect and Size Effect

The ideal bead shape on the tip of thermocouple where it measures the temperature should be a perfect sphere. But in reality, these thermocouple was made more or less likely to be an ellipse rather than a perfect sphere, so it is important to keep in mind this is one of the source where it will cause data error.

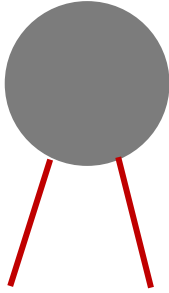
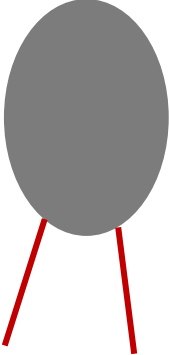
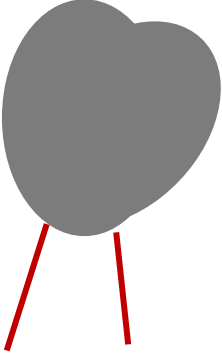
| | | |
|---|---|---|
|  |  |  |
| Ideal Beads | Bad Example 1 | Bad Example 2 |
| Gives uniform conduction and grants measurement accuracy | Bad Shape of Thermocouple beads will lead to conduction delay when taking measurements which will cause non-accurate data be recorded | |

Figure E.1: Sketch of Beads Shape and Effect

For the bead on the tip of the thermocouple, too large or too small are neither the option we want, what we are looking for is the right size. To determine the proper size of the bead, it has to deal with the wire radius and the holes size which we drilled in the experiment. Too large of the bead may causing the bead to pick up temperature reading from our heated metal plate, where too small of the bead will let the thermocouple wire directly exposed to the surrounding and giving our bad reading.

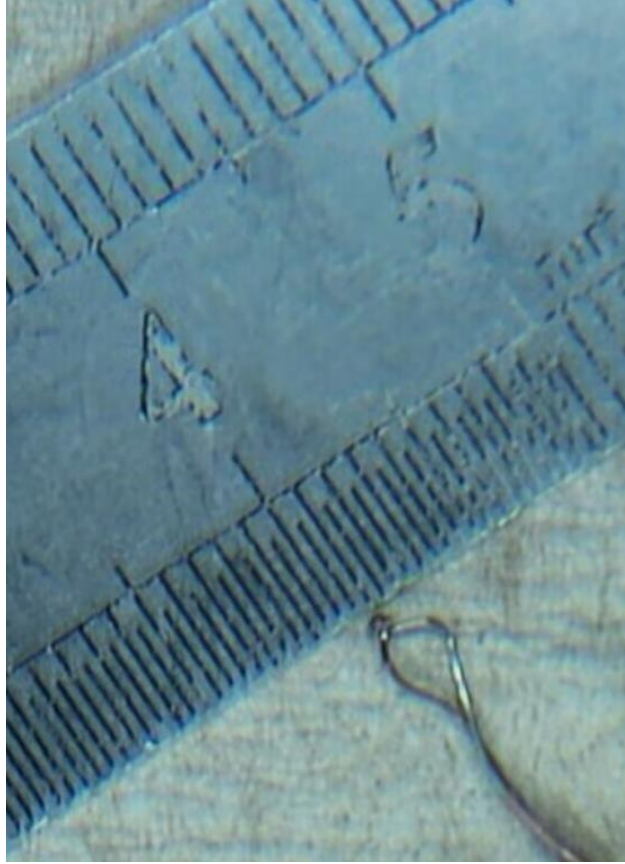


Figure E.2: Picture of Actual Thermocouple Beads

Appendix F. Thermocouple wire length effect

The length of the thermocouple wire does not have to be a finite number. Although it may go as long as possible, but too long will surely not be good. One firm effect of wire length will be resistance, the longer the wire, the resistance and signal travel along the wire will be stack more. Other physical effects such as room temperature may even affect more when the thermocouple wire goes too long.

In this experiment, we tried to keep all of our thermocouple wire to be around 1 meter or 3 feet, to give us some flexibility while moving the container around the data collector but also won't have too much of effect from the environment or wire itself.

Appendix G. Effect by Location of Thermocouple Beads

The thermocouple should not be pushed into the center of the container, but we also don't want it to sit too back in the hole. By pushing thermocouple too far may cause disruption to the flow inside the container where sitting way too back will have more effect from the radiation from the heating plate rather than measuring the actual temp of the liquid.

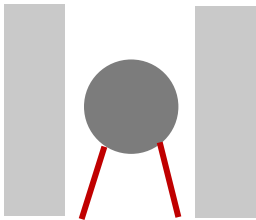
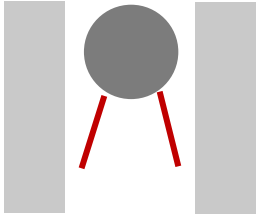
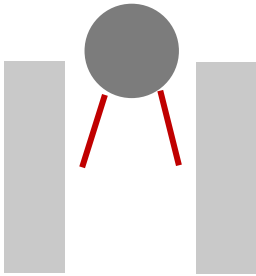
| | | |
|--|---|--|
|  |  |  |
| Beads Too In | Ideal Location | Beads Too Out |
| <p>In this configuration, beads located way to deep in the hole, so it will take longer to measure the temperature of PCM while also being effect a lot by the radiation of the aluminum plate besides it.</p> | <p>In this configuration, beads are measuring the PCM with minimal effect from plates beside it, while also not causing any turbulence to the PCM liquid.</p> | <p>While this configuration will keep beads away from the aluminum plate, it will cause turbulent in the PCM liquid once we start applying mechanical vibration to the container which will leads to data error.</p> |

Figure G.1: Beads Location Effect